

Date of publication xxxx 00, 0000, date of current version xxxx 00, 0000.

Digital Object Identifier 10.1109/ACCESS.2017.Doi Number

# Multibody dynamics model and simulation for the totally enclosed lifeboat lowered from ship in rough seas

Shaoyang Qiu<sup>1</sup>, Hongxiang Ren<sup>1</sup>, Haijiang Li<sup>1</sup>, Yi Zhou<sup>2</sup>, and Delong Wang<sup>1</sup>

<sup>1</sup>Key Laboratory of Marine Dynamic Simulation and Control for Ministry of Communications, Dalian Maritime University, Dalian 116026, China

<sup>2</sup>CNOOC Energy Technology & Service- Oil Production Services Co, Tianjin, 300452, China

Corresponding author: Hongxiang Ren (e-mail: dmu\_rhx@163.com).

The authors thank the financial support provided by National Natural Science Foundation of China (Grant No. 52071312), Liaoning Provincial Natural Science Foundation shipping joint fund project (Grant No. 2020-HYLH-29), Provincial postgraduate education and teaching achievement award cultivation project (Grant No. YJG2020601).

**ABSTRACT** For the design of ship equipment and crew training, it would be useful to develop software for the three-dimensional simulation of a totally enclosed lifeboat. To improve the simulation accuracy and immersion of the software, we present a multibody dynamics model for a lifeboat lowered from a ship, accounting for the coupled motion among the ship, lifeboat slings, a cable-pulley system, and the lifeboat. The equations of the whole system are formulated using Kane's method. The model of ship manoeuvring mathematical group is used to calculate the forces and moments acting on the hull of the ship. The hydrodynamic and wind loads on the boat are modeled using the strip theory. The impact force between the ship and the boat colliding is estimated using the contact theory of Hertz and an elastoplastic model. The method of lumped mass is used to model the lifeboat slings. For the cable-pulley system, we present an efficient model for the dynamics of the pay-out/reel-in process based on the framework of Kane's method. The local load of each cable segment between two pulleys is calculated by the model of a linear spring on the basis of the amount of cable passages over pulleys and the variation of the pulley positions, conversely, the cable segment exerts force and moment on the pulleys. The motion equations of the whole system are solved using fourth-order Runge-Kutta. The model can simulate the lowering of the lifeboat, and obtain the three-dimensional motion parameters of the ship, the lifeboat, slings and pulleys, and the local tension load of the cable. The results show that the simulation curves are near the ones of the model experiment, and their trends are coincident. Thus, it can be concluded that our model is feasible. According to our model, the motion of the ship has a significant effect on the magnitude of the lifeboat's oscillation when the sea state is above level 4; it is safe when the initial clear distance is greater than 1.5 times the width of the boat and the sea conditions are below level 5. Finally, the model is applied to the software for three-dimensional simulation.

**INDEX TERMS** Lifeboat, Lumped mass, Cable-pulley system, Kane's method, Hertzian contact, Simulation.

## I. INTRODUCTION

### A. MOTIVATION

As the main life-saving equipment of ships, a lifeboat undertakes the important task of life-saving when a shipwreck accident occurs. The totally enclosed lifeboats are often located on two sides of the ship. Generally, the boat is equipped with an inverted-boom davit that has a double hanging point. When crews release the lifeboat, at first, the arms of the davit are rotated to outside of the ship, at this

time, the lifeboat arrives in the embarkation position. After the crews enter the lifeboat, the lifeboat is lowered until it reaches the surface of the water. The process of releasing lifeboat mainly includes two phases: the rotation of the arms and lowering the lifeboat. During the rotation of the arms, the crews on board can restrict the large range motion of the lifeboat by a rope to prevent dangerous situations. The operation of lowering the lifeboat together with embarked persons into the water is more hazardous phase in rough seas. The lifeboat, during its lowering from a significant height in

the neighborhood of the rolling ship's side, often impacts against the side. The overloads may lead to serious damage to the hull structure of the lifeboat and threaten the personal safety of the crews [1]–[3].

For this reason, it is necessary to search for an exact method for calculation of the motion parameters of a lifeboat lowered from the ship to the water in rough seas conditions. When a reliable computational software is available, this allows for the improvement of the existing design solutions and testing new solutions of the devices in question. It can also be used to train crews to improve their proficiency in operation and safety awareness. Thus, the authors study a method for that.

The schematic diagram of the lifeboat equipment system is shown in Figure 1. The bow and stern of the lifeboat are connected with the slings. The upper ends of the slings are connected with the movable pulleys. The rest of the pulleys are fixed on the davit that is omitted in the figure. For the convenience of viewing, the number of fixed pulleys in the figure is less than the actual situation. The drum and davit are fixed on the deck. The position and the Euler angle of the davit arm relative to the ship remain unchanged when the lifeboat is being lowered. The whole system only needs to control the speed of the drum to release the cable. The cable is released and the pulleys rotate. The movable pulleys and slings are lowered with the lifeboat. Therefore, we will look for a calculation method to consider the effect of the cable-pulley system, the lifeboat slings, and the ship on the lifeboat.

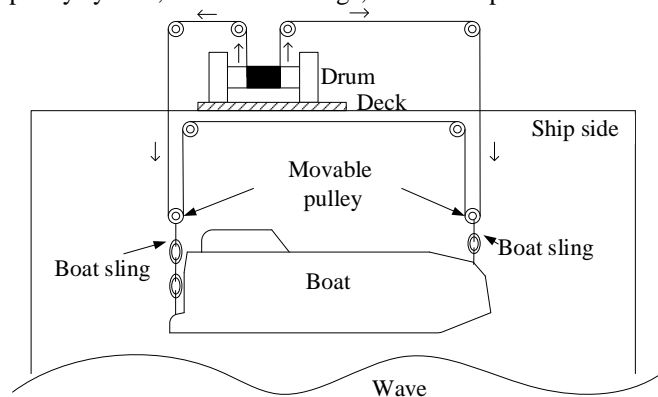


FIGURE 1. Schematic diagram of lifeboat system

## B. RELATED WORK

Re and Veitch [4], [5], Re *et al.* [6], [7] Pelley [8] used a series of model experiments in a large test facility. The performance of a conventional twin-falls davit-launched lifeboat system was evaluated during the evacuation process from a bottom fixed installation. The performance was examined as a function of the weather conditions. Based on the results, some guidance was given concerning the rational design of evacuation system configurations. Magluta *et al.* [9] used simplified physical modeling together with analytical procedures to investigate the dynamic responses of a conventional lifeboat system, suspended from cables. They applied the Lagrange function and Hamilton principle to obtain a system of non-linear differential equations based on

the small-scale model. The equipment of the model experiments was much simpler than that of the actual lifeboat and davit. The motion of the lifeboat was in a two-dimensional plane. They mainly obtained the tension of the cables. Raman-Nair *et al.* [10] used the multi-body dynamics method to establish a motion model for the releasing of the lifeboat from the moving platform into the water, at the same time, the interaction between the lifeboat and the elastic boom was also considered. They comprehensively analyzed the forces acting on the lifeboat and gave the calculation methods of every force and moment. The platform had a simple harmonic motion without the effects of the environment. The cable-pulley system and lifeboat slings were not involved. Ekman [11], [12] presented a numerical model that simulated the lowering of a boat from a ship in beam seas. Since the ship had no forward speed and was exposed to beam seas, a 2-dimensional mathematical model of the ship's motion in waves was provided. The boat's mathematical model was derived based on the Lagrange equation as a simple pendulum system. The effect of wind on the boat was not considered. The numerical results were in good agreement with the experimental tests. Dymarski and Dymarski [13] established a three-dimensional motion model for a lifeboat. This was introduced as a complex model that accounted for sea conditions as well as elasticity and damping properties of davit's elements and mechanisms, rope and lifeboat hull; however, they did not give the specific details of the algorithm. Dymarski *et al.* [14] simplified the model of the ship motion to find the values of the ship motion parameters, which appeared to be the most dangerous for people in the lifeboat due to the generated accelerations. The computational model was derived from the literature [13]. Kniat [15] presented a description of a computer program for the motion visualization of a lifeboat lowered along a ship's side. The program was a post-processor that read the results of numerical calculations of simulated objects' motions. The data was used to create a scene composed of 3D surfaces to visualize the mutual spatial positions of a lifeboat, the ship's sides, and water waving surface. This is only a computer program for 3D visualization without the detailed algorithm.

In summary, the current research regarding the motion model of a lifeboat lowered from a ship in rough seas is limited. The current studies do not involve effective algorithms regarding the actual structure of the davit, such as the cable-pulley system and lifeboat slings that will be of great help in studying the cable overload or breakage in rough seas. Only Ekman's algorithm was compared with the experimental data; however, this was only the boat's motion in a two-dimensional plane.

There is also research on three-dimensional coupled motion derived from the Lagrange equation [16]. However, if we use this method to deduce the coupled motion equation of lifeboat, the ship, and the above complex structure of the davit, the equation will be complicated and difficult to solve.

## C. OUR CONTRIBUTIONS

Kane's method is a practical and effective to calculate and solve complex mechanical systems [17]–[19]. Our contributions are as follows

1) The kinematic equations of the system are formulated using Kane's method.

2) Based on the framework of Kane's method, the model of ship manoeuvring mathematical group (MMG) is used to calculate the motion of the ship in the wave, the method of lumped mass is used to model the lifeboat slings, and the hydrodynamic and wind loads on the lifeboat are modeled using the strip theory. The impact force between the ship and the lifeboat colliding is estimated using the contact theory of Hertz and an elastoplastic model.

3) An efficient model is proposed for the dynamics of the pay-out/reel-in process of the cable-pulley system. The local load of each cable segment between two pulleys is calculated by the model of a linear spring on the basis of the amount of cable passages over pulleys and the variation of the pulley positions, conversely, the cable segment exerts force and moment on the pulleys.

4) The model is applied to software for a three-dimensional simulation of the totally enclosed lifeboat.

The rest of this paper is organized as follows. The multibody dynamics model for the system is in Section 2, we describe the coordinate systems in Section 2.1, the model for the lifeboat in Section 2.2, the model for the ship in Section 2.3, the model for the lifeboat slings in Section 2.4, the model for the multiple pulleys system in Section 2.5, and the kinematic equation in Section 2.6. The results and analysis are discussed in Section 3. The application is in Section 4. The summary is in Section 5.

## II. Multibody dynamics model for the system

### A. COORDINATE SYSTEMS

As shown in Figure 2, there are three Cartesian coordinate systems.  $oxyz$  is an inertial coordinate system with unit vectors of the three axes  $\mathbf{N}_1$ ,  $\mathbf{N}_2$ , and  $\mathbf{N}_3$ .  $o_s x_s y_s z_s$  is a coordinate system fixed to the ship with unit vectors of the three axes  $\mathbf{s}_1$ ,  $\mathbf{s}_2$ , and  $\mathbf{s}_3$ .  $o_s$  is located at the center of gravity.  $\mathbf{s}_1$  points to the bow.  $\mathbf{s}_2$  points to the right of the ship.  $\mathbf{s}_3$  points the keel.  $o_b x_b y_b z_b$  is the lifeboat coordinate system, with unit vectors of the three axes  $\mathbf{b}_1$ ,  $\mathbf{b}_2$ , and  $\mathbf{b}_3$ .  $o_b$  is located at the center of gravity for the lifeboat.

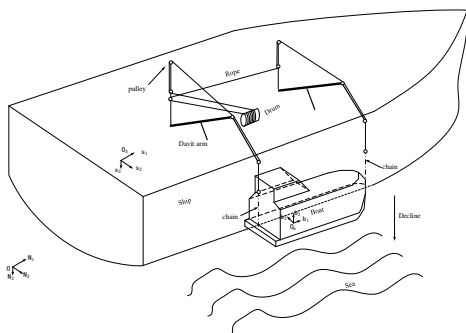


FIGURE 2. Schematic diagram of three coordinate systems.

### B. LIFEBOAT

When a lifeboat is lowered, it is affected by the gravity, the wind drag and lift, the fluid drag, the buoyancy, the tension of the slings, and the contact force with the ship.

The rotation transformation matrix of the lifeboat coordinate system and inertial coordinate system is  ${}^N C^b$ .

$$\begin{pmatrix} \mathbf{N}_1 \\ \mathbf{N}_2 \\ \mathbf{N}_3 \end{pmatrix} = [{}^N C^b] \begin{pmatrix} \mathbf{b}_1 \\ \mathbf{b}_2 \\ \mathbf{b}_3 \end{pmatrix} \quad (1)$$

$$[{}^N C^b] = \begin{pmatrix} c_2 c_3 & s_1 s_2 c_3 - s_3 c_1 & c_1 s_2 c_3 + s_3 s_1 \\ c_2 s_3 & s_1 s_2 s_3 + c_1 c_3 & c_1 s_2 s_3 - c_3 s_1 \\ -s_2 & s_1 c_2 & c_1 c_2 \end{pmatrix} \quad (2)$$

where  $s_i = \sin \theta_i^b$ ,  $c_i = \cos \theta_i^b$  ( $i = 1, 2, 3$ ), and  $\theta_i^b$  is the angle between the lifeboat coordinate system and inertial coordinate system.

Define the generalized coordinates as

$$\begin{cases} q_i^b = \theta_i^b \\ q_{3+i}^b = \overline{OO_b} \cdot \mathbf{b}_i \end{cases} \quad (i = 1, 2, 3) \quad (3)$$

The generalized velocities are

$$\begin{cases} u_i^b = \boldsymbol{\omega}^b \cdot \mathbf{b}_i \\ u_{3+i}^b = \mathbf{v}^b \cdot \mathbf{b}_i \end{cases} \quad (i = 1, 2, 3) \quad (4)$$

where  $\boldsymbol{\omega}^b$  and  $\mathbf{v}^b$  are the velocity and angular velocity of the lifeboat, respectively.

The relationships between the generalized coordinates and generalized velocities are [20]

$$\begin{cases} \dot{q}_1^b = u_1^b + s_2 / c_2 (u_2^b s_1 + u_3^b c_1) \\ \dot{q}_2^b = u_2^b c_1 - u_3^b s_1 \\ \dot{q}_3^b = (u_2^b s_1 + u_3^b c_1) / c_2 \end{cases} \quad (5)$$

$$\begin{cases} \dot{q}_4^b = u_4^b - u_2^b q_6^b + u_3^b q_5^b \\ \dot{q}_5^b = u_5^b + u_1^b q_6^b - u_3^b q_4^b \\ \dot{q}_6^b = u_6^b - u_1^b q_5^b + u_2^b q_4^b \end{cases} \quad (6)$$

The angular acceleration and acceleration of the lifeboat are

$$\boldsymbol{\alpha}^b = \sum_{i=1}^3 \dot{u}_i^b \mathbf{b}_i \quad (7)$$

$$\begin{cases} \mathbf{a}^b \cdot \mathbf{b}_1 = \dot{u}_4^b + u_2^b u_6^b - u_3^b u_5^b \\ \mathbf{a}^b \cdot \mathbf{b}_2 = \dot{u}_5^b - u_1^b u_6^b + u_3^b u_4^b \\ \mathbf{a}^b \cdot \mathbf{b}_3 = \dot{u}_6^b + u_1^b u_5^b - u_2^b u_4^b \end{cases} \quad (8)$$

The partial angular velocities and velocities of the lifeboat are

$$\omega_r^b = \begin{cases} \mathbf{b}_r & (r=1,2,3) \\ 0 & (r=4,5,6) \end{cases} \quad (9)$$

$$\mathbf{v}_r^b = \begin{cases} 0 & (r=1,2,3) \\ \mathbf{b}_{r-3} & (r=4,5,6) \end{cases} \quad (10)$$

The generalized inertial force is

$$F_r^{*b} = \begin{cases} -[\dot{u}_1^b I_1 - u_2^b u_3^b (I_2 - I_3)] \\ -[\dot{u}_2^b I_2 - u_3^b u_1^b (I_3 - I_1)] \\ -[\dot{u}_3^b I_3 - u_1^b u_2^b (I_1 - I_2)] \\ -m_b (\dot{u}_4^b + u_2^b u_6^b - u_3^b u_5^b) \\ -m_b (\dot{u}_5^b - u_1^b u_6^b + u_3^b u_4^b) \\ -m_b (\dot{u}_6^b + u_1^b u_5^b - u_2^b u_4^b) \end{cases} \quad (11)$$

where  $I_1, I_2$ , and  $I_3$  are the rotational moment of inertia around axis  $ox_b, oy_b$ , and  $oz_b$ ; and  $m_b$  is the lifeboat mass.

Equation (11) can be written as follows.

$$\{F^{*b}\} = -[V^b]\{\dot{u}^b\} - [W^b]\{\phi^b\} \quad (12)$$

where  $[V^b]$  and  $[W^b]$  are a  $6 \times 6$  diagonal matrix, and its elements are  $V_{11}^b = I_1, V_{22}^b = I_2, V_{33}^b = I_3, V_{44}^b = V_{55}^b = V_{66}^b = m_b, W_{11}^b = I_3 - I_2, W_{22}^b = I_1 - I_3, W_{33}^b = I_2 - I_1$  and  $W_{44}^b = W_{55}^b = W_{66}^b = m_b$ . Vector  $\{\dot{u}^b\}$  is a  $6 \times 1$  column vector, and its elements are  $\dot{u}_r^b (r=1, \dots, 6)$ .  $\{\phi^b\}$  is a  $6 \times 1$  column vector element,  $\phi_1^b = u_2^b u_3^b, \phi_2^b = u_3^b u_1^b, \phi_3^b = u_1^b u_2^b, \phi_4^b = u_2^b u_6^b - u_3^b u_5^b, \phi_5^b = u_3^b u_4^b - u_1^b u_6^b$ , and  $\phi_6^b = u_1^b u_5^b - u_2^b u_4^b$ .

The generalized force caused by the gravity of the lifeboat is

$$F_r^{G^b} = m_b g \mathbf{N}_3 \cdot \mathbf{v}_r^b \quad (13)$$

where  $g$  is the acceleration of gravity.

The generalized force caused by wind drag is

$$F_r^{W^b} = \mathbf{F}_b^W \cdot \mathbf{v}_r^b \quad (14)$$

$$\mathbf{F}_b^W = -\frac{1}{2} \rho_w A_w^b C_w^b |\mathbf{v}^{b/w}| \mathbf{v}^{b/w} \quad (15)$$

where  $\mathbf{v}^{b/w}$  is vector difference between the lifeboat velocity and wind velocity,  $\mathbf{v}^{b/w} = \mathbf{v}^b - \mathbf{v}^w$ ,  $\rho_w$  is the density of air,  $A_w^b$  is the projected area of the surface of the lifeboat in the plane perpendicular to  $\mathbf{v}^{b/w}$ , and  $C_w^b$  is the wind drag coefficient.

To determine the wind lift, we modeled the lifeboat as a cylinder with diameter  $D_b$  and length  $l_b$ . The length is parallel to  $\mathbf{b}_1$ . The wind lift  $\mathbf{F}_b^L$  is [10]

$$\mathbf{F}_b^L = -\frac{1}{2} \rho_w D_b l_b C_L^b |\mathbf{v}_n^{b/w}|^2 \mathbf{k} \quad (16)$$

where  $C_L^b$  is the lift coefficient,  $\mathbf{v}_n^{b/w} = (u_5^b - v_2^{w/w})\mathbf{b}_2 + (u_6^b - v_3^{w/w})\mathbf{b}_3$ ,  $v_i^{w/w}$  is the component of wind velocity  $\mathbf{v}^w$  in the direction of  $\mathbf{b}_i$ , and  $\mathbf{k} = \mathbf{b}_1 \times \mathbf{v}_n^{b/w} / |\mathbf{b}_1 \times \mathbf{v}_n^{b/w}|$  is the direction vector.

$$F_r^{L^b} = \mathbf{F}_b^L \cdot \mathbf{v}_r^b \quad (17)$$

The lifeboat is divided into  $n$  cross sections of equal thickness along the length direction  $\mathbf{b}_1$ , the coordinates of the centre of each cross section  $s_k (k=1, \dots, n)$  are expressed in the lifeboat coordinate system as  $(x_{s_k}, 0, 0)$ . The thickness of each cross section is  $t_s = l_b / n$ . The generalized force caused by fluid drag is

$$F_r^{D^b} = \sum_{k=1}^n F_r^{D^b/s_k} (r=1, \dots, 6) \quad (18)$$

$$F_r^{D^b/s_k} = \mathbf{F}_{s_k}^D \cdot \mathbf{v}_r^{s_k} \quad (19)$$

where  $\mathbf{F}_{s_k}^D$  is the fluid drag acting on each section, and  $\mathbf{v}_r^{s_k}$  is partial velocity of each cross section with components  $v_1^{s_k} = u_4, v_2^{s_k} = u_5 + x_{s_k} u_3$  and  $v_3^{s_k} = u_6 + x_{s_k} u_2$  in  $\mathbf{b}_i$ .

The partial velocities of each section are

$$\mathbf{v}_r^{s_k} = \begin{cases} 0 & (r=1) \\ -x_{s_k} \mathbf{b}_3 & (r=2) \\ x_{s_k} \mathbf{b}_2 & (r=3) \\ \mathbf{b}_{r-3} & (r=4,5,6) \end{cases} \quad (20)$$

The components of the fluid resistance acting on each section are

$$\mathbf{F}_{s_k}^D = \sum_{i=1}^3 D_i^{s_k} \mathbf{b}_i \quad (21)$$

$$\begin{cases} D_1^{s_k} = -\frac{1}{2n} \rho_a A_1^{s_k} c_{D_1}^{s_k} |v_1^{s_k/R}| v_1^{s_k/R} \\ D_2^{s_k} = -\frac{1}{2} \rho_a A_2^{s_k} c_{D_2}^{s_k} |v_2^{s_k/R}| v_2^{s_k/R} \\ D_3^{s_k} = -\frac{1}{2} \rho_a A_3^{s_k} c_{D_3}^{s_k} |v_3^{s_k/R}| v_3^{s_k/R} \end{cases} \quad (22)$$

where  $\rho_a$  is the density of seawater,  $A_i^{s_k}$  is the area of the section  $s_k$  perpendicular to  $\mathbf{b}_i$  below the water surface, the section  $s_m$  has maximum area  $A_1^{s_k} = \max(A_i^{s_k}) (k=1 \dots n)$ ,  $c_{D_i}^{s_k}$  is the coefficient of friction, and  $v_i^{s_k/R}$  is the component of

the velocity of the section  $s_k$  relative to the wave surface on the axis of  $\mathbf{b}_i$ .

The buoyancy of lifeboat is

$$\mathbf{F}^{B/b} = \sum_{k=1}^n \rho_a V_{s_k} g \mathbf{N}_3 \quad (23)$$

where  $V_{s_k}$  is the volume of each cross section in the water, and the moment caused by buoyancy is  $\mathbf{T}^{B/b}$  with component  $T_i^{B/b}$  in  $\mathbf{b}_i$ .

$$\begin{cases} T_1^{B/b} = \sum_{k=1}^n \rho_a V_{s_k} g h_m \sin \Omega \\ T_2^{B/b} = \sum_{k=1}^n \rho_a V_{s_k} g x_{s_k} \cos \Omega \\ T_3^{B/b} = \sum_{k=1}^n \rho_a V_{s_k} g x_{s_k} \sin \Omega \end{cases} \quad (24)$$

where  $h_m$  is the metacentric height as shown in Figure 3.

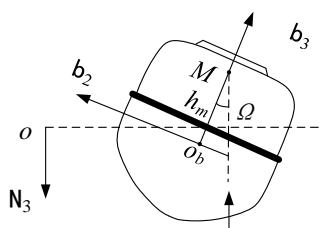


FIGURE 3. Buoyancy moment and metacentric height of Lifeboat's roll.

The generalized force caused by buoyancy is

$$F_r^{B/b} = \mathbf{F}^{B/b} \cdot \mathbf{v}_r^b + \mathbf{T}^{B/b} \cdot \boldsymbol{\omega}_r^b \quad (25)$$

The hanging points attached the lifeboat in the lifeboat coordinate system are  $p_0^\alpha (a_1^\alpha, a_2^\alpha, a_3^\alpha) (\alpha=1,2)$ . The generalized force caused by the slings  $F_r^{T/b}$  is

$$F_r^{T/b} = \begin{cases} \sum_{\alpha=1}^2 (a_2^\alpha \mathbf{b}_3 - a_3^\alpha \mathbf{b}_2) \mathbf{F}_{p_0}^\alpha & (r=1) \\ \sum_{\alpha=1}^2 (a_3^\alpha \mathbf{b}_1 - a_1^\alpha \mathbf{b}_3) \mathbf{F}_{p_0}^\alpha & (r=2) \\ \sum_{\alpha=1}^2 (a_1^\alpha \mathbf{b}_2 - a_2^\alpha \mathbf{b}_1) \mathbf{F}_{p_0}^\alpha & (r=3) \\ \sum_{\alpha=1}^2 \mathbf{b}_1 \mathbf{F}_{p_0}^\alpha & (r=4) \\ \sum_{\alpha=1}^2 \mathbf{b}_2 \mathbf{F}_{p_0}^\alpha & (r=5) \\ \sum_{\alpha=1}^2 \mathbf{b}_3 \mathbf{F}_{p_0}^\alpha & (r=6) \end{cases} \quad (26)$$

where the force of the slings acting on the lifeboat is  $\mathbf{F}_{p_0}^\alpha = (f_{i,1}^\alpha + r_{i,1}^\alpha) \cdot d_{i,1}^\alpha \mathbf{b}_i$ , and the definition and calculation of  $\mathbf{F}_{p_0}^\alpha, f_{i,1}^\alpha, r_{i,1}^\alpha, d_{i,1}^\alpha$  is in the Section 2.4.

The lifeboat, during its lowering in the neighborhood of rolling ship's side, often impacts against the side of the ship. As shown in Figure 4, there are two anti-collision devices attached to the lifeboat's hull. The lifeboat collides with the ship through the anti-collision devices. The impact process consists of a compression phase and a restitution phase. For the compression phase, we use the well-known Hertzian contact law to calculate the contact stresses [21].

The Hertzian theory assumes that the contacting surfaces are non-conforming and for determining local deformations each body is regarded as an elastic half space loaded over a small elliptical region. In this way, the highly concentrated contact stresses are independent of the general stress distribution in the bodies arising from their shape and other external influences. Denote the Young's modulus and Poisson's ratio of the ship and lifeboat by  $E_s, \nu_s$  and  $E_b, \nu_b$  respectively, and the radius of curvature of the surface of the ship and lifeboat at the point of contact by  $R_s, R_b$ . Denoting the relative indentation or penetration between the contacting bodies by  $\delta$ , the magnitude of the contact force in the compression phase is [21].

$$f^c = K \delta^{3/2} \quad (27)$$

where  $K = \frac{4}{3} E^* R^{1/2}$ ,  $E^* = \left( \frac{1-\nu_s^2}{E_s} + \frac{1-\nu_b^2}{E_b} \right)^{-1}$ , and  $R = R_s R_b / (R_s + R_b)$ .

We address problems in which the energy loss due to impact results in local permanent plastic deformation. For the restitution phase, therefore, we use the contact force model of Lankarani and Nikravesh [22], [23]. They denote the local permanent plastic deformation by  $\delta_p$  which is related to the coefficient of restitution, the impact velocity, and the material properties. The magnitude of the contact force in this phase is

$$f^c = f_m^c \left( \frac{\delta - \delta_p}{\delta - \delta_m} \right)^{3/2} \quad (28)$$

where  $f_m^c = K^{2/5} (5m_t \dot{\delta}_0^2 / 4)^{3/5}$ ,  $m_t = m_b + m_s$ ,  $m_b$  and  $m_s$  are the mass of the lifeboat and ship,  $\dot{\delta}_0$  is the relative impact speed at  $\delta=0$ ,  $\delta_m = (5m_t \dot{\delta}_0^2 / 4K)^{2/5}$ ,  $\delta_p = 5m_t \dot{\delta}_0^2 (1 - e_r^2) / 4f_m^c$ , and  $e_r$  is the coefficient of restitution.

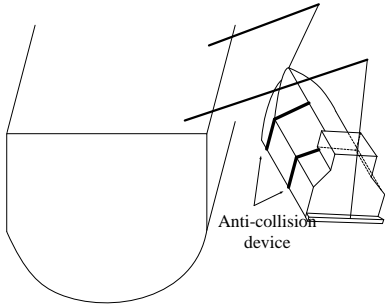


FIGURE 4. Schematic diagram of anti-collision device attached to the lifeboat's hull.

The ship's hull surface is assumed to be a plane in this paper as shown in Figure 5. The plane's equation is  $A_s x + B_s y + C_s z + D_s = 0$ . The coefficients  $(A_s, B_s, C_s, D_s)$  can be obtained from any three points in the plane that are not in a straight line. The outer normal vector of the plane is  $\vec{n}_s(A_s, B_s, C_s)$ . The anti-collision devices are divided into  $n_d$  points  $p_i^d (i=1, \dots, n_d)$  with the coordinates  $({}^b x_i^d, {}^b y_i^d, {}^b z_i^d)$  in the lifeboat coordinate system, the  $({}^N x_i^d, {}^N y_i^d, {}^N z_i^d)$  in the inertial coordinate system, and the  $({}^s x_i^d, {}^s y_i^d, {}^s z_i^d)$  in the ship coordinate system. The transformations of the coordinates are

$$\begin{Bmatrix} {}^b x_i^d \\ {}^b y_i^d \\ {}^b z_i^d \end{Bmatrix} = - \begin{Bmatrix} q_4^b \\ q_5^b \\ q_6^b \end{Bmatrix} + [{}^N C^b]^T \begin{Bmatrix} {}^N x_i^d \\ {}^N y_i^d \\ {}^N z_i^d \end{Bmatrix} \quad (i=1, \dots, n_d) \quad (29)$$

$$\begin{Bmatrix} {}^b x_i^d \\ {}^b y_i^d \\ {}^b z_i^d \end{Bmatrix} = - \begin{Bmatrix} q_4^b \\ q_5^b \\ q_6^b \end{Bmatrix} + [{}^N C^b]^T [{}^N C^s] \begin{Bmatrix} q_4^s + {}^s x_i^d \\ q_5^s + {}^s y_i^d \\ q_6^s + {}^s z_i^d \end{Bmatrix} \quad (i=1, \dots, n_d) \quad (30)$$

where  $[{}^N C^s]$  is the rotation transformation matrix between the ship's coordinate system and inertial coordinate system,  $q_i^s$  are the generalized coordinates of the ship.

The distance between each point and the ship is  $D_i^p$

$$D_i^p = \left| A_s {}^N x_i^d + B_s {}^N y_i^d + C_s {}^N z_i^d \right| / \sqrt{A_s^2 + B_s^2 + C_s^2} \quad (31)$$

For the point  $p_i^d$ , defining a variable  $\sigma_i^d(t)$

$$\sigma_i^d(t) = A_s {}^N x_i^d + B_s {}^N y_i^d + C_s {}^N z_i^d + D_s \quad (32)$$

When  $\sigma_i^d(t) \cdot \sigma_i^d(0) < 0$ , the point  $p_i^d$  contacts with the ship,  $\delta_i = D_i^p$ , and the relative impact speed  $\dot{\delta}$  can be calculated by

$$\dot{\delta} = \left( \mathbf{v}^s + \boldsymbol{\omega}^s \times \begin{Bmatrix} {}^s x_i^d \mathbf{s}_1 \\ {}^s y_i^d \mathbf{s}_2 \\ {}^s z_i^d \mathbf{s}_3 \end{Bmatrix} - \mathbf{v}^b - \boldsymbol{\omega}^b \times \begin{Bmatrix} {}^b x_i^d \mathbf{b}_1 \\ {}^b y_i^d \mathbf{b}_2 \\ {}^b z_i^d \mathbf{b}_3 \end{Bmatrix} \right) \cdot \vec{n}_s \quad (33)$$

where  $\mathbf{v}^s$  and  $\boldsymbol{\omega}^s$  are the velocity and angular velocity of the ship, respectively. The contact force  $f_i^c$  can be calculated using (27,28). The generalized force caused by the impact force is

$$F_r^{Cb} = \begin{cases} \sum_{i=1}^{n_d} ({}^b y_i^d \mathbf{b}_3 - {}^b z_i^d \mathbf{b}_2) f_i^c \vec{n}_s & (r=1) \\ \sum_{i=1}^{n_d} ({}^b z_i^d \mathbf{b}_1 - {}^b x_i^d \mathbf{b}_3) f_i^c \vec{n}_s & (r=2) \\ \sum_{i=1}^{n_d} ({}^b x_i^d \mathbf{b}_2 - {}^b y_i^d \mathbf{b}_1) f_i^c \vec{n}_s & (r=3) \\ \sum_{i=1}^{n_d} \mathbf{b}_1 f_i^c \vec{n}_s & (r=4) \\ \sum_{i=1}^{n_d} \mathbf{b}_2 f_i^c \vec{n}_s & (r=5) \\ \sum_{i=1}^{n_d} \mathbf{b}_3 f_i^c \vec{n}_s & (r=6) \end{cases} \quad (34)$$

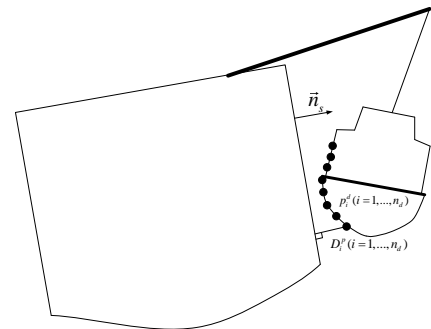


FIGURE 5. Schematic diagram of calculating contact force in this paper, the anti-collision devices are divided into  $n_d$  points, the distance between each point and the ship is  $D_i^p$ .

### C. SHIP

The force and moment of the ship's body are based on the model of the MMG. The interferential forces and moments of the regular wave and the wind are regarded as a part of external forces. In order to solve the system equation conveniently, the equations of ship motion are written as follows

Define the generalized coordinates as

$$\begin{cases} q_i^s = \theta_i^s & (i=1,2,3) \\ q_{3+i}^s = \overline{OO_s} \cdot \mathbf{s}_i \end{cases} \quad (35)$$

The generalized velocities are

$$\begin{cases} u_i^s = \boldsymbol{\omega}^s \cdot \mathbf{s}_i & (i=1,2,3) \\ u_{3+i}^s = \mathbf{v}^s \cdot \mathbf{s}_i \end{cases} \quad (36)$$

where  $\theta_i^s$  are the Euler angles of ship in the inertial coordinate system.

The partial angular velocities and velocities of the ship are

$$\omega_r^s = \begin{cases} \mathbf{s}_r & (r=1,2,3) \\ 0 & (r=4,5,6) \end{cases} \quad (37)$$

$$\mathbf{v}_r^s = \begin{cases} 0 & (r=1,2,3) \\ \mathbf{s}_{r-3} & (r=4,5,6) \end{cases} \quad (38)$$

The relationship between the generalized coordinates and generalized velocities, acceleration, angular acceleration and generalized inertial force  $F_r^{*s}$  of the ship are expressed in the same way as with the lifeboat. The generalized inertial force  $F_r^{*s}$  can also be written in the form of (12). The rotation transformation matrix between the ship's coordinate system and inertial coordinate system is  $[{}^N C^s]$ . Each element in  $[{}^N C^s]$  is calculated by (2) replacing  $\theta_i^b$  with  $\theta_i^s$ . The generalized force of the ship is

$$F_r^{S/s} = \mathbf{F}^{S/s} \cdot \mathbf{v}_r^s + \mathbf{T}^{S/s} \cdot \omega_r^s \quad (39)$$

The calculation of the force and moment of the ship are based on the model of the MMG [24]. The coordinate system is shown in Figure 2. Considering the environmental forces, the forces acting on ship are

$$\mathbf{F}^{S/s} = \begin{cases} (X_H + X_{wind} + X_{wave})\mathbf{s}_1 \\ (Y_H + Y_{wind} + Y_{wave})\mathbf{s}_2 \\ (Z_H + Z_{wind} + Z_{wave})\mathbf{s}_3 \end{cases} \quad (40)$$

$$\mathbf{T}^{S/s} = \begin{cases} (K_H + K_{wind} + K_{wave})\mathbf{s}_1 \\ (M_H + M_{wind} + M_{wave})\mathbf{s}_2 \\ (N_H + N_{wind} + N_{wave})\mathbf{s}_3 \end{cases} \quad (41)$$

where the variables with subscript H are the force and moment acting on the hull, and the variables with subscript wind, wave are the force and moment of wind and wave.

For the wave force, it is estimated based on the assumption of Froude–Krylov, where the hull is simplified to a box, and the six-degree-of-freedom wave force and moment are clearly stated in [25] and [26].

$$\begin{cases} X_{wave} \\ Y_{wave} \\ Z_{wave} \\ K_{wave} \\ M_{wave} \\ N_{wave} \end{cases} = \rho_a g \zeta e^{-kd} \sin(\epsilon B) \begin{cases} \frac{2d}{E} \sin(FL) \sin(\omega_e t + \epsilon) \\ -\frac{2dl}{FB} \sin(FL) \sin(\omega_e t + \epsilon) \\ \frac{kd}{Eq} \sin(FL) \cos(\omega_e t + \epsilon) \\ \frac{d^2}{FB} \sin(FL) \sin(\omega_e t + \epsilon) \\ \frac{d}{2EF^2} (\sin(FL) - FL \cos(FL)) \sin(\omega_e t + \epsilon) \\ \frac{d}{kF^2} (\sin(FL) - FL \cos(FL)) \cos(\omega_e t + \epsilon) \end{cases} \quad (42)$$

where  $\zeta$  is the amplitude of wave,  $k$  is the number of wave,  $\omega_e$  is the encounter frequency,  $\epsilon$  is initial phase,  $E = 0.5k \sin \chi$ ,  $F = 0.5k \cos \chi$ ,  $\chi$  is the encounter angle,  $L$

is the length of the ship's waterline,  $l = \sqrt{c}L$  is the equivalent ship length,  $c$  is the block coefficient,  $B$  is the ship width, and  $d$  is the draught.

Wave can be divided into regular wave and irregular wave. The regular wave can be regarded as a simple harmonic curve composed of a single frequency. However, the irregular wave often has strong randomness [27]. Due to the randomness of wind, the actual sea surface usually presents as short-crested irregular wave.

$$\eta = \sum_{i=1}^n \sum_{j=1}^m \sqrt{2R(\omega_i, \gamma_j) \Delta\omega \Delta\gamma} \cos(\omega_i t + \epsilon_{i,j} - k_i(x \cos(\gamma_j) + y \sin(\gamma_j))) \quad (43)$$

where  $R(\omega, \chi) = S(\omega)D$  is the directional wave spectral density function [28],  $S(\omega)$  is the frequency spectrum function,  $D$  is directional spreading function [29],  $\Delta\gamma = \gamma_j - \gamma_0$ .  $\gamma_0$  is main wave direction,  $\Delta\gamma$  is the difference between wave direction  $\gamma_j$  and  $\gamma_0$ . The frequency spectrum function of China's coastal areas is

$$S(\omega) = 0.74 \omega^{-5} \exp(-g^2 / (U^2 \omega^2)) \quad (44)$$

where  $U$  is wind speed, which can be approximated by  $U = 6.28\sqrt{H}$ ,  $H$  is the height of significant wave, the interval of  $\omega$  is (0.3, 3) [30].

$$D = \begin{cases} \frac{2^{2s-1} s! (s-1)!}{\pi (2s-1)!} \cos^{2s}(\Delta\gamma) & \Delta\gamma < \frac{\pi}{2} \\ 0 & \text{otherwise} \end{cases} \quad (45)$$

where the interval of  $\gamma_j$  is  $(\gamma_0 - 30^\circ, \gamma_0 + 30^\circ)$  [28]. The simulation diagram of irregular wave is shown in Figure 6.

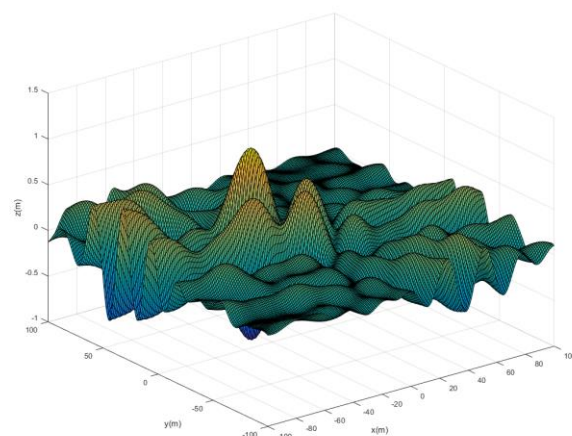


FIGURE 6. The simulation diagram of irregular waves .

The force and moment of a ship in irregular waves can be regarded as the linear superposition of the wave force and moment of a ship in regular waves with different frequencies and amplitudes refers to (42).

The wind force and moment are generally reflected in the ship's horizontal and rolling motions. Ignoring the effect on heave and pitch, the wind force and moment are [24]

$$\begin{cases} X_{\text{wind}} = \frac{1}{2} \rho_w A_{w1}^s (\mathbf{v}^{w/s})^2 C_{wx}^s(\alpha_R) \\ Y_{\text{wind}} = \frac{1}{2} \rho_w A_{w2}^s (\mathbf{v}^{w/s})^2 C_{wy}^s(\alpha_R) \\ K_{\text{wind}} = Y_{\text{wind}} h_z \\ N_{\text{wind}} = \frac{1}{2} \rho_w A_{w2}^s L_{oa} (\mathbf{v}^{w/s})^2 C_{wn}^s(\alpha_R) \end{cases} \quad (46)$$

where  $C_{wx}^s(\alpha_R)$ ,  $C_{wy}^s(\alpha_R)$ , and  $C_{wn}^s(\alpha_R)$  are the coefficients of the wind pressure,  $\alpha_R$  is the relative bearing of the wind,  $\mathbf{v}^{w/s} = \mathbf{v}^w - \mathbf{v}^s$ ,  $h_z$  is the height of the action point of the wind force,  $A_{w1}^s$  and  $A_{w2}^s$  are the projected area in the forward and lateral direction above the waterline of the ship, and  $L_{oa}$  is the overall length of the ship.

#### D. LIFEBOAT SLINGS

There are two slings connected with the lifeboat. The upper end of each sling is connected to the movable pulley, and the lower end is connected to the lifeboat. Based on the framework of Kane's method, they are modeled by the spring-mass model [31]–[33]. As shown in Figure 7, there are  $n$  particles  $p_j^\alpha$  ( $j=1, \dots, n; \alpha=1, 2$ ) at each sling with mass  $m_{p_j^\alpha}$ . The motion of each particle is three degrees of freedom, and its generalized coordinates and velocities are

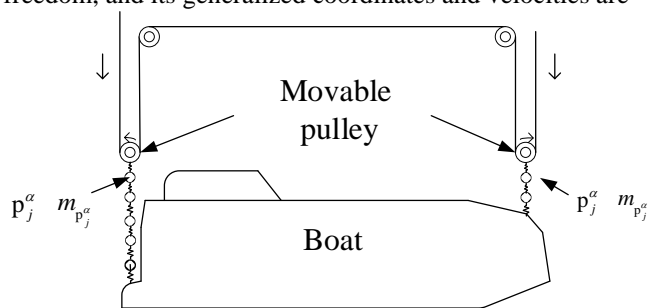


FIGURE 7. Schematic diagram of the slings attached the lifeboat, the slings are modeled by the spring-mass model.

$$q_{3j-3+i}^\alpha = \overline{p_0^\alpha p_j^\alpha} \mathbf{b}_i \quad (i=1, 2, 3; j=1, \dots, n; \alpha=1, 2) \quad (47)$$

$$\mathbf{v}_{3j-3+i}^\alpha = \mathbf{v}_{p_j^\alpha}^\alpha \mathbf{b}_i \quad (i=1, 2, 3; j=1, \dots, n; \alpha=1, 2) \quad (48)$$

where  $p_0^\alpha (a_1^\alpha, a_2^\alpha, a_3^\alpha)$  are the lower ends of the slings attached to the lifeboat, and the  $\mathbf{v}_{p_j^\alpha}^\alpha$  is the velocity.

Define  $L_{i,0}^\alpha = a_i^\alpha$ . The coordinates of each particle in the lifeboat coordinate system are

$$L_{i,j}^\alpha = L_{i,0}^\alpha + q_{3j-3+i}^\alpha \quad (i=1, 2, 3; j=1, \dots, n; \alpha=1, 2) \quad (49)$$

${}^s h_i^\alpha$ ,  ${}^b h_i^\alpha$  are the position coordinates of the movable pulley in the ship coordinate system and the lifeboat coordinate system. Their transformation relationship refers to (30).

Thus,

$$L_{i,n+1}^\alpha = {}^b h_i^\alpha \quad (i=1, 2, 3; \alpha=1, 2) \quad (50)$$

The relationship between the generalized coordinates and generalized velocities is [20]

$$\begin{cases} \dot{q}_{3j-2}^\alpha = u_{3j-2}^\alpha - (u_4^b + u_2^b L_{3,j}^\alpha - u_3^b L_{2,j}^\alpha) \\ \dot{q}_{3j-1}^\alpha = u_{3j-1}^\alpha - (u_5^b + u_3^b L_{1,j}^\alpha - u_1^b L_{3,j}^\alpha) \\ \dot{q}_{3j}^\alpha = u_{3j}^\alpha - (u_6^b + u_1^b L_{2,j}^\alpha - u_2^b L_{1,j}^\alpha) \end{cases} \quad (j=1, \dots, n; \alpha=1, 2) \quad (51)$$

The generalized inertial force is [20]

$$\begin{cases} F_{3j-2}^{*\alpha} = -m_{p_j^\alpha} (\dot{u}_{3j-2}^\alpha + u_2^b u_{3j}^\alpha - u_3^b u_{3j-1}^\alpha) \\ F_{3j-1}^{*\alpha} = -m_{p_j^\alpha} (\dot{u}_{3j-1}^\alpha - u_1^b u_{3j}^\alpha + u_3^b u_{3j-2}^\alpha) \\ F_{3j}^{*\alpha} = -m_{p_j^\alpha} (\dot{u}_{3j}^\alpha + u_1^b u_{3j-1}^\alpha - u_2^b u_{3j-2}^\alpha) \end{cases} \quad (j=1, \dots, n; \alpha=1, 2) \quad (52)$$

The generalized inertial force can be written as follows

$$\{F^{*\alpha}\} = -[V^\alpha] \{\dot{u}^\alpha\} - [V^\alpha] \{\phi^\alpha\} \quad (53)$$

where  $[V^\alpha]$  is a  $3n \times 3n$  diagonal matrix, its elements are  $V_{3j-2,3j-2}^\alpha = V_{3j-1,3j-1}^\alpha = V_{3j,3j}^\alpha = m_{p_j^\alpha}$ , vector  $\{\dot{u}^\alpha\}$  is a  $3n \times 1$  column vector, and its elements are  $\dot{u}_r^\alpha$ ,  $\{\phi^\alpha\}$  is a  $3n \times 1$  column vector, and its element  $\phi_{3j-2}^\alpha = u_2^b u_{3j}^\alpha - u_3^b u_{3j-1}^\alpha$ ,  $\phi_{3j-1}^\alpha = -u_1^b u_{3j}^\alpha + u_3^b u_{3j-2}^\alpha$ , and  $\phi_{3j}^\alpha = u_1^b u_{3j-1}^\alpha - u_2^b u_{3j-2}^\alpha$ .

The generalized force caused by the gravity of each particle is

$$\begin{cases} F_{3j-2}^{G/\alpha} = m_{p_j^\alpha} g (\sin - q_2^b) \\ F_{3j-1}^{G/\alpha} = -m_{p_j^\alpha} g (\sin q_1^b \cos q_2^b) \\ F_{3j}^{G/\alpha} = -m_{p_j^\alpha} g (\cos q_1^b \cos q_2^b) \end{cases} \quad (j=1, \dots, n; \alpha=1, 2) \quad (54)$$

Define

$$d_{i,j}^\alpha = L_{i,j}^\alpha - L_{i,j-1}^\alpha \quad (i=1, 2, 3; j=1, \dots, n+1; \alpha=1, 2) \quad (55)$$

$$D_{1,j}^\alpha = \sqrt{\sum_{i=1}^3 (d_{i,j}^\alpha)^2} \quad (i=1, 2, 3; j=1, \dots, n+1; \alpha=1, 2) \quad (56)$$

$$D_{2,j}^\alpha = D_{1,j}^\alpha - l^\alpha / (n+1) \quad (57)$$

where  $l^\alpha$  is the initial length of the sling  $\alpha$ . The elastic force of each spring is calculated based on the model of a linear spring.

$$f_{1,j}^\alpha = k_j^\alpha D_{2,j}^\alpha / D_{1,j}^\alpha \quad (j=1, \dots, n+1; \alpha=1,2) \quad (58)$$

where  $k_j^\alpha$  is the spring constant of the  $j$ -th segment,  $k_j^\alpha = A^\alpha E^\alpha (n+1)/l^\alpha$ ,  $A^\alpha$  is the area of the cross-section, and  $E^\alpha$  is the modulus of elasticity.

$$\begin{cases} f_{2,j}^\alpha = f_{1,j+1}^\alpha \\ f_{3,j}^\alpha = -f_{1,j}^\alpha \end{cases} \quad (j=1, \dots, n; \alpha=1,2) \quad (59)$$

The generalized force caused by the spring elastic force is

$$\begin{cases} F_{3j-2}^{S/\alpha} = (f_{2,j}^\alpha d_{1,j+1}^\alpha + f_{3,j}^\alpha d_{1,j}^\alpha) \\ F_{3j-1}^{S/\alpha} = (f_{2,j}^\alpha d_{2,j+1}^\alpha + f_{3,j}^\alpha d_{2,j}^\alpha) \\ F_{3j}^{S/\alpha} = (f_{2,j}^\alpha d_{3,j+1}^\alpha + f_{3,j}^\alpha d_{3,j}^\alpha) \end{cases} \quad (j=1, \dots, n; \alpha=1,2) \quad (60)$$

The velocity vector difference between two particles is

$$v_{i,j}^\alpha = (\mathbf{v}_{p_j}^\alpha - \mathbf{v}_{p_{j-1}}^\alpha) \mathbf{b}_i \quad (i=1,2,3; j=1, \dots, n+1; \alpha=1,2) \quad (61)$$

$$\mathbf{v}_{p_0}^\alpha = \begin{cases} (u_4^b + u_2^b a_3^\alpha - u_3^b a_2^\alpha) \mathbf{b}_1 \\ (u_5^b + u_3^b a_1^\alpha - u_1^b a_3^\alpha) \mathbf{b}_2 \\ (u_6^b + u_1^b a_2^\alpha - u_2^b a_1^\alpha) \mathbf{b}_3 \end{cases} \quad (62)$$

where  $\mathbf{v}_{p_{n+1}}^\alpha$  is the velocity of the movable pulley. The spring structure damping is based on the model of a linear spring.

$$r_{1,j}^\alpha = c^\alpha v_{i,j}^\alpha \text{sign}(D_{2,j}^\alpha) / D_{1,j}^\alpha \quad (j=1, \dots, n+1; \alpha=1,2) \quad (63)$$

where  $c^\alpha$  is the damping coefficient.

$$\begin{cases} r_{2,j}^\alpha = r_{1,j+1}^\alpha \\ r_{3,j}^\alpha = -r_{1,j}^\alpha \end{cases} \quad (j=1, \dots, n; \alpha=1,2) \quad (64)$$

The generalized force caused by the spring damping force

$$\begin{cases} F_{3j-2}^{R/\alpha} = (r_{2,j}^\alpha d_{1,j+1}^\alpha + r_{3,j}^\alpha d_{1,j}^\alpha) \\ F_{3j-1}^{R/\alpha} = (r_{2,j}^\alpha d_{2,j+1}^\alpha + r_{3,j}^\alpha d_{2,j}^\alpha) \\ F_{3j}^{R/\alpha} = (r_{2,j}^\alpha d_{3,j+1}^\alpha + r_{3,j}^\alpha d_{3,j}^\alpha) \end{cases} \quad (j=1, \dots, n; \alpha=1,2) \quad (65)$$

## E. MULTIPLE PULLEYS SYSTEM

Ju and Choo [34] presented a parametric super element model for a cable passing through multiple pulleys. The amounts of cable passages over pulleys were introduced as additional degrees-of-freedom in the finite element model and the relationship between the cable tensions at the two sides of each pulley was imposed based on the friction law or empirical data. The model was applied to the static analysis of structures. García-Fernández *et al.* [35] proposed a model for the dynamics of a cable passing through a set of pulleys and an oscillation model based on the classical one-dimensional wave equation. The load of the cable segments was taken into account; however, the load of every cable segment was the same. Kamman and Huston [36] presented

a procedure for studying the dynamics of variable length cable systems in deployment and retrieval (pay-out and reel-in) without pulleys. In this paper, the variable length of the cable and local load should be considered. There are some accurate algorithms [37]–[39]. They can meet our requirements in terms of the calculation accuracy, but they are time-consuming and cannot guarantee the real-time performance. We presented a model considering the forces and moments that appear on these pulleys, and the local load of the cable segments, as well as the variable length of cable in real time based on Ju and Choo [34].

As shown in Figure 8, a cable passes through multiple pulleys. There are  $n$  nodes,  $n-1$  segments of cable, and  $n-2$  pulleys. One segment of cable is shown in Figure 9. Our algorithm assumes that there is no slip between the cable and the pulleys, and does not consider the complex situation of cable bending under stress [40]. The elastic deformation in each segment is caused by rotation and displacement of the pulleys. The elastic tension of the cable has an effect on the motion of the pulley.

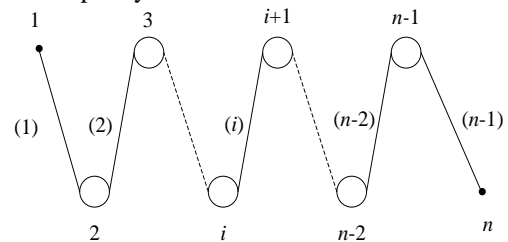


FIGURE 8. Multiple pulleys system.

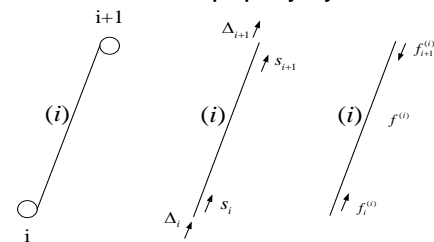


FIGURE 9.  $i$ -th segment of system.

The change in the length of each segment is

$$\Delta l_{(i)} = \left| \overline{p_i p_{i+1}} \right| - \left| \overline{p_i p_{i+1}} \right| \quad (66)$$

where  $\left| \overline{p_i p_{i+1}} \right| = \left| \overline{p_i p_{i+1}} + \Delta_{i+1} - \Delta_i \right|$ ,  $p_i$  is the node position,  $\Delta_i$  is the node displacement,  $k^{(i)}$  is the spring constant, and  $s_i$  is the length of the cable passed through the node  $i$ . The local load of the cable  $i$  is based on the model of a linear spring

$$f^{(i)} = k^{(i)} (s_{i+1} - s_i + \Delta l_{(i)}) \quad (67)$$

$$\begin{cases} f_{i+1}^{(i)} \\ f_i^{(i)} \end{cases} = \begin{cases} f^{(i)} \\ f^{(i)} \end{cases} \quad (68)$$

The vector of force

$$\begin{cases} \mathbf{F}_{i+1}^{(i)} \\ \mathbf{F}_i^{(i)} \end{cases} = \begin{bmatrix} -\lambda^{(i)} & 0 \\ 0 & \lambda^{(i)} \end{bmatrix} \begin{cases} f_{i+1}^{(i)} \\ f_i^{(i)} \end{cases} \quad (69)$$

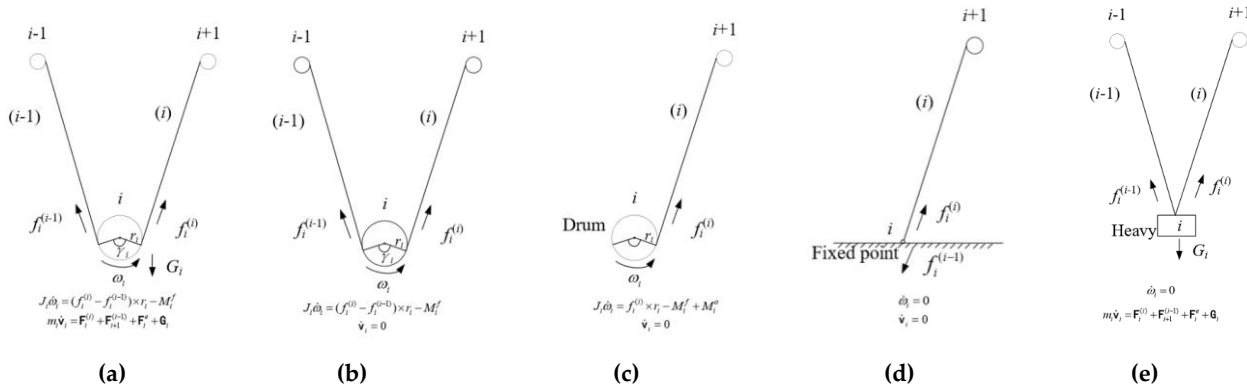


FIGURE 10. Five types of nodes and their calculation of motion (a) Movable pulley, (b) Fixed pulley, (c) Cable drum, (d) Fixed point, (e) Heavy.

$J_i = 1/2 m_i r_i^2$  is the rotational inertia,  $r_i$  is the radius,  $m_i$  is the mass,  $\omega_i$  is the angular velocity,  $\dot{s}_i = \omega_i \times r_i$ ,  $M_i^f$  is the frictional moment,  $M_i^a$  is the active torque,  $\mathbf{G}_i$  is the vector of gravity,  $\mathbf{v}_i$  is the vector of velocity, and  $\mathbf{F}_i^e$  is the vector of the external force.

Lowering the totally enclosed lifeboat involves the node type of movable pulley, fixed pulley, and cable drum. The motion of the fixed pulley and the drum is one degree of freedom, and the motion of the movable pulley is four degrees of freedom.

The total number of pulleys and drums is  $m$ . Define the generalized coordinates and velocities

$$\begin{cases} q_i^p = \theta_i^p \\ u_i^p = \dot{\theta}_i^p \end{cases} (i = 1, 2, \dots, m) \quad (70)$$

The generalized force

$$\mathbf{F}_i^{vp} = ((f_i^{(i)} - f_{i+1}^{(i-1)}) \times r_i \times c_i^\gamma - M_i^f + M_i^a) \quad (71)$$

where  $c_i^\gamma$  is a coefficient that is related to the contact angle  $\gamma_i$  between the cable and the pulley. This paper approximates it as  $c_i^\gamma = \gamma_i / \pi$ . The unit of  $\gamma_i$  is radians.

The generalized inertial force is

$$\mathbf{F}_i^{*p} = -J_i \dot{u}_i^p \quad (72)$$

Equation (72) can be written as follows

$$\{\mathbf{F}^{*p}\} = -[V^p] \{\dot{u}^p\} \quad (73)$$

where  $[V^p]$  is an  $m \times m$  diagonal matrix,  $V_{i,i}^p = J_i$ .  $\{\dot{u}^p\}$  is a  $m \times 1$  column vector, and its elements are  $\dot{u}_i^p$ .

where  $\lambda_x^{(i)} = (x_{i+1} - x_i) / l_{(i)}$ ,  $\lambda_y^{(i)} = (y_{i+1} - y_i) / l_{(i)}$ ,  $\lambda_z^{(i)} = (z_{i+1} - z_i) / l_{(i)}$ ,  $\lambda^{(i)} = [\lambda_x^{(i)} \lambda_y^{(i)} \lambda_z^{(i)}]$ .  $x_i$ ,  $y_i$ , and  $z_i$  are coordinates of the node.

There are five types of system nodes. A solution of the node's motion is shown in Figure 10.

In addition to the rotation of the movable pulley, it also has translational motion of three degrees of freedom. The two movable pulleys are  $p_{n+1}^\alpha$  ( $\alpha = 1, 2$ ), and the transformation relationship between the two movable pulleys in the coordinate system of lifeboat and ship refers to (30). The generalized coordinates and generalized velocities are

$$q_{3n+i}^\alpha = \overline{p_0^\alpha p_{n+1}^\alpha} \mathbf{b}_i (i = 1, 2, 3; \alpha = 1, 2) \quad (74)$$

$$u_{3n+i}^\alpha = \mathbf{v}_{p_{n+1}^\alpha} \mathbf{b}_i (i = 1, 2, 3; \alpha = 1, 2) \quad (75)$$

Thus,

$$L_{i,n+1}^\alpha = L_{i,0}^\alpha + q_{3n+i}^\alpha (i = 1, 2, 3; \alpha = 1, 2) \quad (76)$$

$$\begin{cases} \dot{q}_{3n+1}^\alpha = u_{3n+1}^\alpha - (u_4^b + u_2^b L_{3,n+1}^\alpha - u_3^b L_{2,n+1}^\alpha) \\ \dot{q}_{3n+2}^\alpha = u_{3n+2}^\alpha - (u_5^b + u_3^b L_{1,n+1}^\alpha - u_1^b L_{3,n+1}^\alpha) (\alpha = 1, 2) \\ \dot{q}_{3n+3}^\alpha = u_{3n+3}^\alpha - (u_6^b + u_1^b L_{2,n+1}^\alpha - u_2^b L_{1,n+1}^\alpha) \end{cases} \quad (77)$$

The generalized force caused by the gravity

$$\begin{cases} F_{3n+1}^{G/\alpha} = m_{p_{n+1}^\alpha} g (\sin - q_2^b) \\ F_{3n+2}^{G/\alpha} = -m_{p_{n+1}^\alpha} g (\sin q_1^b \cos q_2^b) (\alpha = 1, 2) \\ F_{3n+3}^{G/\alpha} = -m_{p_{n+1}^\alpha} g (\cos q_1^b \cos q_2^b) \end{cases} \quad (78)$$

The generalized force caused by the cable on both sides of the pulley

$$\begin{cases} \mathbf{F}_{3n+1}^{1/\alpha} = ({}^a \mathbf{F}_i^{(i)} + {}^a \mathbf{F}_{i+1}^{(i-1)}) \mathbf{b}_1 \\ \mathbf{F}_{3n+2}^{1/\alpha} = ({}^a \mathbf{F}_i^{(i)} + {}^a \mathbf{F}_{i+1}^{(i-1)}) \mathbf{b}_2 (\alpha = 1, 2) \\ \mathbf{F}_{3n+3}^{1/\alpha} = ({}^a \mathbf{F}_i^{(i)} + {}^a \mathbf{F}_{i+1}^{(i-1)}) \mathbf{b}_3 \end{cases} \quad (79)$$

The generalized force caused by the spring of the slings

$$\begin{cases} F_{3n+1}^{S/\alpha} \\ F_{3n+2}^{S/\alpha} \\ F_{3n+3}^{S/\alpha} \end{cases} = \begin{cases} -f_{1,n+1}^\alpha d_{1,n+1}^\alpha \\ -f_{1,n+1}^\alpha d_{2,n+1}^\alpha \\ -f_{1,n+1}^\alpha d_{3,n+1}^\alpha \end{cases} \quad (80)$$

The generalized force caused by the damping force of the slings

$$\begin{cases} F_{3n+1}^{R/\alpha} \\ F_{3n+2}^{R/\alpha} \\ F_{3n+3}^{R/\alpha} \end{cases} = \begin{cases} -r_{1,n+1}^\alpha d_{1,n+1}^\alpha \\ -r_{1,n+1}^\alpha d_{2,n+1}^\alpha \\ -r_{1,n+1}^\alpha d_{3,n+1}^\alpha \end{cases} \quad (81)$$

The generalized inertial force

$$\begin{cases} F_{3n+1}^{*\alpha} = -m_{\rho_{n+1}}^\alpha (\dot{u}_{3n+1}^\alpha + u_2^b u_{3n+3}^\alpha - u_3^b u_{3n+2}^\alpha) \\ F_{3n+2}^{*\alpha} = -m_{\rho_{n+1}}^\alpha (\dot{u}_{3n+2}^\alpha - u_1^b u_{3n+3}^\alpha + u_3^b u_{3n+1}^\alpha) (\alpha = 1, 2) \\ F_{3n+3}^{*\alpha} = -m_{\rho_{n+1}}^\alpha (\dot{u}_{3n+3}^\alpha + u_1^b u_{3n+2}^\alpha - u_2^b u_{3n+1}^\alpha) \end{cases} \quad (82)$$

Equation (82) can also be written in the form of (53).

### F. KINEMATIC EQUATION

For the entire system, the lifeboat and the ship have six degrees of freedom respectively, the rotation of the pulley and the drum have  $m$  degrees of freedom, and there are  $6n+6$  degrees of freedom for the displacement of the mass particles and the movable pulleys. The entire system has  $6n+m+18$  degrees of freedom. The generalized coordinates, generalized velocity, generalized force and generalized inertial force of the system are  $\bar{q}_i$ ,  $\bar{u}_i$ ,  $\bar{F}_i$ , and  $\bar{F}_i^*$  ( $i=1, \dots, 6n+m+12$ ), respectively. Define  $t=12+m, h=t+3n+3, w=h+3n+3$ .

$$\bar{q}_i = \begin{cases} q_i^b & (i=1, \dots, 6) \\ q_{i-1}^s & (i=7, \dots, 12) \\ q_{i-12}^p & (i=13, \dots, t) \\ q_{i-t}^{\alpha=1} & (i=t+1, \dots, h) \\ q_{i-h}^{\alpha=2} & (i=h+1, \dots, w) \end{cases} \quad (83)$$

$$\bar{u}_i = \begin{cases} u_i^b & (i=1, \dots, 6) \\ u_{i-1}^s & (i=7, \dots, 12) \\ u_{i-12}^p & (i=13, \dots, t) \\ u_{i-t}^{\alpha=1} & (i=t+1, \dots, h) \\ u_{i-h}^{\alpha=2} & (i=h+1, \dots, w) \end{cases} \quad (84)$$

$$\bar{F}_i = \begin{cases} F_i^b & (i=1, \dots, 6) \\ F_{i-1}^s & (i=7, \dots, 12) \\ F_{i-12}^p & (i=13, \dots, t) \\ F_{i-t}^{\alpha=1} & (i=t+1, \dots, h) \\ F_{i-h}^{\alpha=2} & (i=h+1, \dots, w) \end{cases} \quad (85)$$

where  $F^b = F^{G/b} + F^{D/b} + F^{W/b} + F^{L/b} + F^{B/b} + F^{T/b} + F^{C/b}$ ,

$$F^s = F^{S/s}, F^p = F^{v/p}, F^\alpha = F^{G/\alpha} + F^{S/\alpha} + F^{R/\alpha} + F^{t/\alpha}.$$

$$\bar{F}_i^* = \begin{cases} F_i^{*b} & (i=1, \dots, 6) \\ F_i^{*s} & (i=7, \dots, 12) \\ F_{i-12}^{*p} & (i=13, \dots, t) \\ F_{i-t}^{*\alpha=1} & (i=t+1, \dots, h) \\ F_{i-h}^{*\alpha=2} & (i=h+1, \dots, w) \end{cases} \quad (86)$$

The generalized inertial force is

$$\{\bar{F}_i^*\} = -[V]\{\dot{\bar{u}}\} - [W]\{\phi\} \quad (87)$$

where  $[V] = \text{diag}([V^b], [V^s], [V^p], [V^{\alpha=1}], [V^{\alpha=2}])$ ,  $[W] = \text{diag}([W^b], [W^s], [W^p], [W^{\alpha=1}], [W^{\alpha=2}])$ ,  $\{\phi\} = \{\{\phi^b\}', \{\phi^s\}', \{\phi^p\}', \{\phi^{\alpha=1}\}', \{\phi^{\alpha=2}\}'\}'$ . The elements in  $[W^p]$  and  $\{\phi^p\}$  are zero.

The system motion equation is

$$\{\bar{F}_i^*\} + \{\bar{F}_i\} = \{0\} \quad (88)$$

According to the (88)

$$\{\dot{\bar{u}}\} = [V]^{-1}(-[W]\{\phi\} + \{\bar{F}\}) \quad (89)$$

Define the column vector as

$$\{x\} = \begin{Bmatrix} \{\bar{q}\} \\ \{\bar{u}\} \end{Bmatrix} \quad (90)$$

The system motion equation can be solved by

$$\{\dot{x}\} = \begin{Bmatrix} \{\dot{\bar{q}}\} \\ \{\dot{\bar{u}}\} \end{Bmatrix} \quad (91)$$

where  $\{\dot{\bar{q}}\}$  can be solved by fourth-order Runge-Kutta according to (5,6,51,77), and the omitted ship motion formula,  $\{\dot{\bar{u}}\}$  can be solved by fourth-order Runge-Kutta according to (89).

## III. RESULTS AND ANALYSIS

### A. COMPARISON WITH MODLE EXPERIMENTS

The basic dimensions of the lifeboat are in accordance with [4]. A 1:13 scale model of a generic 80 person totally enclosed lifeboat was used in the experiments. The lifeboat is lowered from a fixed platform with a lowering speed 1.1 m/s [7]. The lifeboat's length, maximum width, and maximum height are 0.769, 0.285, and 0.277m, respectively. The lifeboat's mass is 5.38kg. The air drag coefficient is 0.07, the fluid drag coefficient is 0.08, the lift coefficient 0.08, and the initial metacentric height of the lifeboat is

$h_m=0.2m$ . All elastic cables have a diameter of 1 mm and an elastic modulus of 10 GPa.

For the convenience of analysis and understanding, the data of the lifeboat's position of simulation in this paper are shown in the new coordinate system  $oxy_1z_1$ , which is obtained by rotating the inertial coordinate system  $180^\circ$  around the  $ox$  axis. For the convenience of comparison, the initial position of the lifeboat is moved to  $(0,0,35)$ .

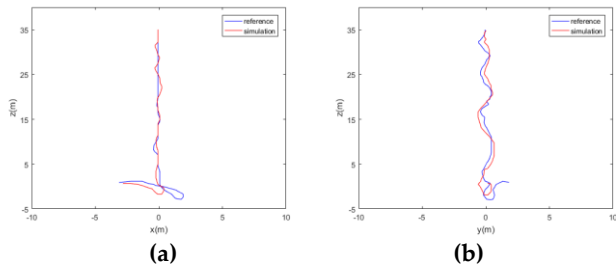


FIGURE 11. Trajectories of the lifeboat in [6] and simulation results under the wind speed 12.2m/s with the orientation of  $-N_1$  and the wave height 4m (a) is trajectories of the ship in  $oxz_1$  plane, (b) is trajectories of the ship in  $oxy_1z_1$  plane.

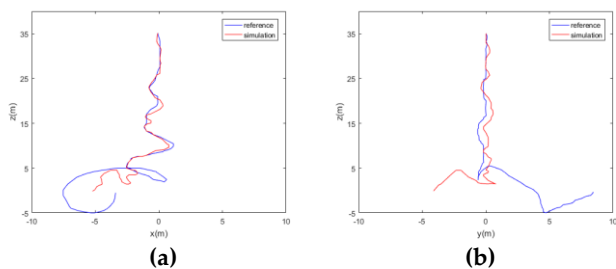


FIGURE 12. Trajectories of the lifeboat in [6] and simulation results under the wind speed 18.5m/s with the orientation of  $-N_2$  and the wave height 9.6m (a) is trajectories of the ship in  $oxz_1$  plane, (b) is trajectories of the ship in  $oxy_1z_1$  plane.

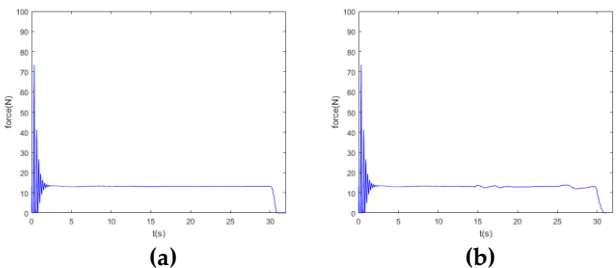


FIGURE 13. The tension of one section of cable in the simulation experiment 1 (a) and 2 (b), the tension of other sections is consistent with that in the figure, only the peak value of tension at the beginning is slightly different.

Comparing the two results in Figures 11 and 12, the trajectories of the lifeboat in the air are relatively close. In Figures 11a and 11b, the maximum errors of the trajectory curve in the air are 0.31m and 0.5m, respectively. In Figures 12a and 12b, the maximum errors of the trajectory curve in the air are 0.51m and 0.62m, respectively. The trajectories of

the lifeboat on the wave have a big gap, as it is difficult to ensure that the position of the lifeboat landing on the wave surface is consistent between the simulation experiment and the model experiment.

As shown in Figures 13, the tension of one section of cable is unstable at first, and it is stable at about 2.5 seconds. The cable tension fluctuates slightly in the stable state. The stable value is about one fourth of the lifeboat's gravity, because there are two movable pulleys in the system. It shows that our model for the cable-pulley system is feasible.

## B. EXPERIMENTS AND QUALITATIVE ANALYSIS

The basic information of the ship is shown in Table 1. The lifeboat's length, maximum width, and maximum height are 11.5, 2.8, and 3.1m. The mass of lifeboat is 8500 kg. The moments of inertia are 25020, 51745, and 51745  $kg \cdot m^2$ . The projected areas of lifeboat normal to the three coordinate axes are 8.5, 26.2, and 26.2  $m^2$ . The air drag coefficient is 0.5, the fluid drag coefficient is 1.2, the lift coefficient is 1.2, and initial metacentric height of the lifeboat is  $h_m=2$  m. The initial distance between the center of the mass of lifeboat and the plane of  $N_1-N_2$  is 15 m. All elastic cables have a diameter of 20 mm and an elastic modulus of 200 GPa. The ship's initial position is  $(0,0,0)$  with the initial velocity  $(0,0,0)$ . The coefficient of restitution is 0.8, the Poisson's ratios of lifeboat and ship are 0.45 and 0.6, respectively. The young's modulus of the lifeboat and ship are 55 GPa and 200 GPa. Figure 14 is initial layout of the ship, davit, and lifeboat. The initial distance between the lifeboat and the ship is half the width of the lifeboat.

TABLE 1. BASIC INFORMATION OF SHIP

Item (unit)	Value
Length over all (m)	139.8
Waterline length (m)	130.55
Length between perpendiculars (m)	126
Width (m)	20.8
Draft (m)	4.4
Depth moulded (m)	11.4
GM (m)	5.57
Distance between center of gravity and center (m)	2.3
Block coefficient	0.68
Water plane coefficient	0.83
Prismatic coefficient	0.693
Displacement (kg)	7550000

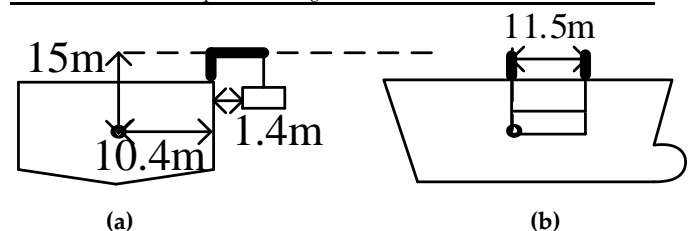


FIGURE 14. The initial layout of ship, davit and lifeboat, (a) is Cross section, (b) is longitudinal section in center plane.

The Levels of sea state from 1 to 5 are calm-rippled, smooth-wavelet, slight, moderate and rough. At level 1 to 3 sea states, releasing a lifeboat is common in the actual operation of navigation. At level 4 and 5 sea states, releasing

a lifeboat has a risk. Therefore, the environmental conditions are set as level 4 and 5 sea state, the wave encounter angles are respectively 0, 45°, 90°, 135°, and 180°. The speed of the drum releasing cable is 0.7m/s [7]. Figures 15 and 16 show the trajectories of the lifeboat when the wave height is 2.5m, and the velocity of wind is 8 m/s (Level 4 sea state). Figures 17 and 18 show the trajectories of the lifeboat when wave height is 4m, velocity of wind is 10m/s (Level 5 sea state). The direction of steady wind is the same as the wave direction. The wave surface is known as a Stokes second-order wave.

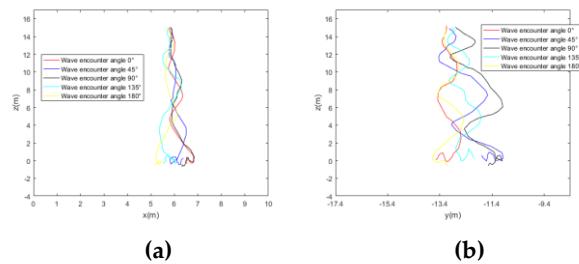


FIGURE 15. The trajectories of the lifeboat at the Level 4 sea state without wind, (a) is the projection of trajectories in  $ox_1z_1$  plane, (b) is the projection of trajectories in  $oy_1z_1$  plane.

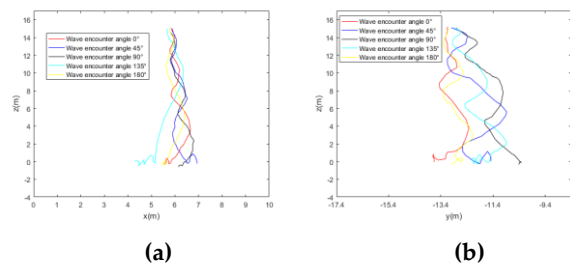


FIGURE 16. The trajectories of the lifeboat at the Level 4 sea state with wind, (a) is the projection of trajectories in  $ox_1z_1$  plane, (b) is the projection of trajectories in  $oy_1z_1$  plane.

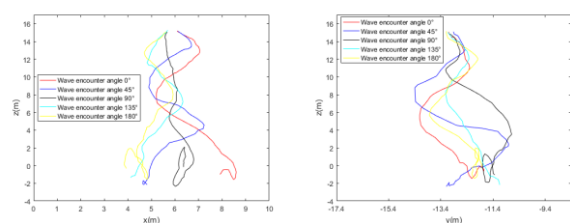


FIGURE 17. The trajectories of the lifeboat at the Level 5 sea state without wind, (a) is the projection of trajectories in  $ox_1z_1$  plane, (b) is the projection of trajectories in  $oy_1z_1$  plane.

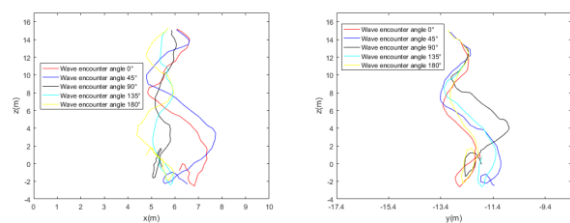


FIGURE 18. The trajectories of the lifeboat at the Level 5 sea state with wind, (a) is the projection of trajectories in  $ox_1z_1$  plane, (b) is the projection of trajectories in  $oy_1z_1$  plane.

The initial position of the boundary of the ship's side plane is -10.5 in the  $oy_1$  axis. Oscillations can be seen to have occurred during lowering as the lifeboat swung as a pendulum. Some of these oscillations may be attributable to the direct forcing by the wind; however, this is mainly due to the motions of the floating ship by the waves according to the comparison of the amplitudes of trajectories' oscillations with wind and without wind. The amplitudes of the oscillations are almost not affected by the wind. The motion of the ship has a significant effect on the lifeboat when the sea state is above level 4. This is consistent with the conclusion of the model test [41].

There are four experiments occurring collision. According to the acceleration curve in Figure 19 at the level 4 sea state, the lifeboat collides with the ship when the wave encounter angle is 90°, at the level 5 sea state, the lifeboat collides with the ship when the wave encounter angles are 45°, 90°, and 135°. The extreme value of the four curves is the acceleration produced by the collision in the horizontal direction. When the wave encounter angle is 90°, the acceleration produced by the collision is greater. Thus, when the wave is closer to the cross wave, the lifeboat is more likely to collide with the ship, and the acceleration caused by collision is greater.

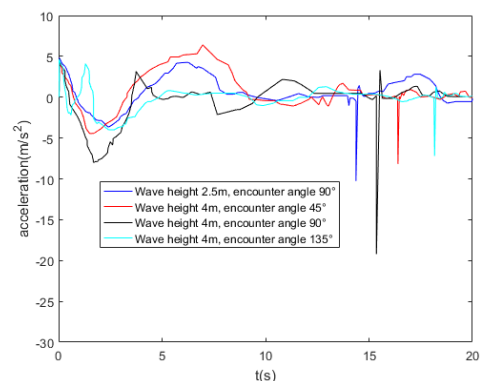


FIGURE 19. Acceleration curves of the lifeboat in the horizontal direction in four experiments

Whether the collision occurs or not also depends on the initial distance between the lifeboat and the ship. The initial distance of the above experiment is half the width of the lifeboat. 100 simulation experiments are conducted for initial distances of 1 time, 1.5 times, and 2 times the lifeboat width in regular waves at level 4 and 5 sea states, and the initial phase of the wave is random. 100 simulation experiments are conducted for same initial distances in irregular waves with significant wave heights of 2.5m and 4m. The minimum distance of per experiment between the lifeboat and ship in regular waves is shown in the Figures 20 and 21, and in irregular waves is shown in the Figures 22 and 23.

The minimum distance between the lifeboat and ship in regular waves with 90° encounter angle is slightly less than that in irregular waves with 90° encounter angle of main wave direction. The minimum distance between the lifeboat and ship in regular waves with 45° and 135° encounter

angles greater than that in irregular waves with  $45^\circ$  and  $135^\circ$  encounter angles of main wave direction. Under the condition of  $90^\circ$  encounter angle, the collision is likely to happen. It is safe if the initial distance is greater than 1.5

times the width of the lifeboat when the sea condition is below level 5.

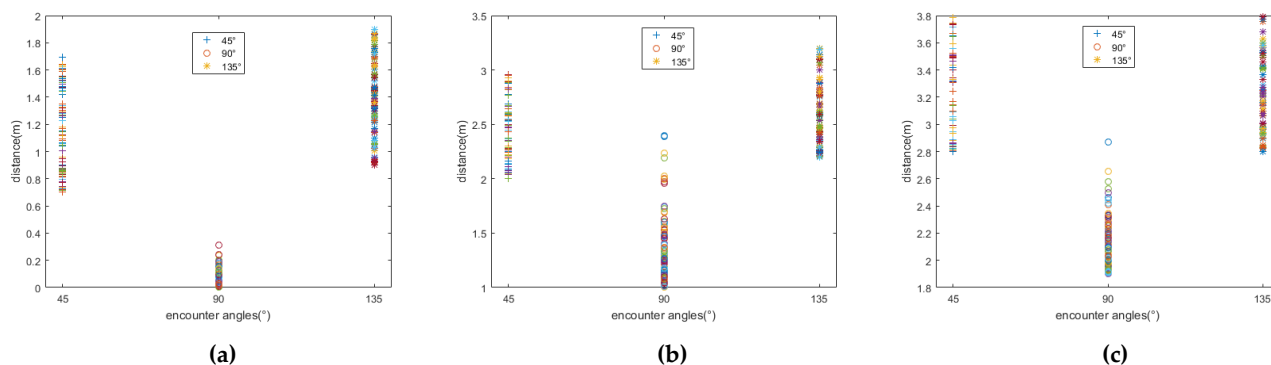


**FIGURE 20.** The shortest distance between lifeboat and ship side at level 4 sea state with initial distance of 1 time (a), 1.5 times (b), and 2 times (c) of lifeboat width. The horizontal ordinates respectively represent encounter angles  $45^\circ$ ,  $90^\circ$ ,  $135^\circ$ , and the longitudinal coordinates is the distance.

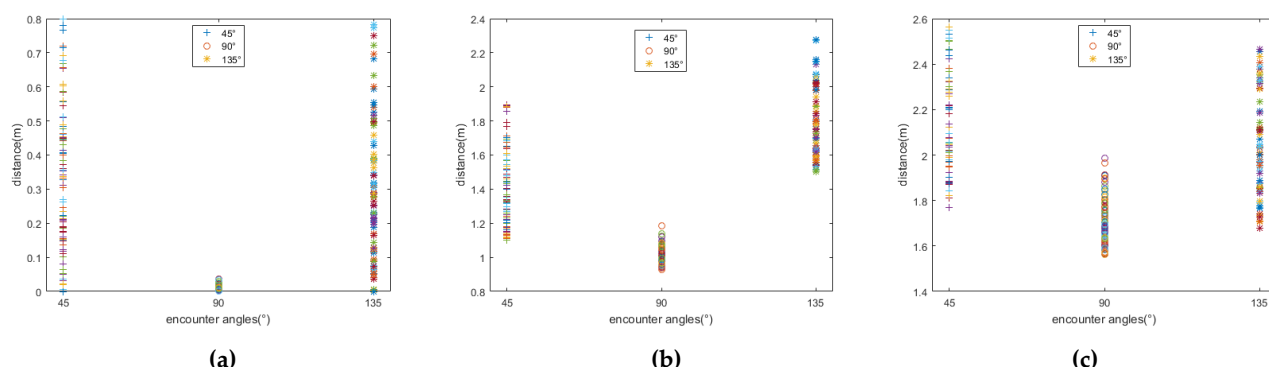


**FIGURE 21.** The shortest distance between lifeboat and ship side at level 5 sea state with initial distance of 1 time (a), 1.5 times (b), and 2 times (c) of lifeboat width. The horizontal ordinates respectively represent encounter angles  $45^\circ$ ,  $90^\circ$ ,  $135^\circ$ , and the longitudinal coordinates is the distance.

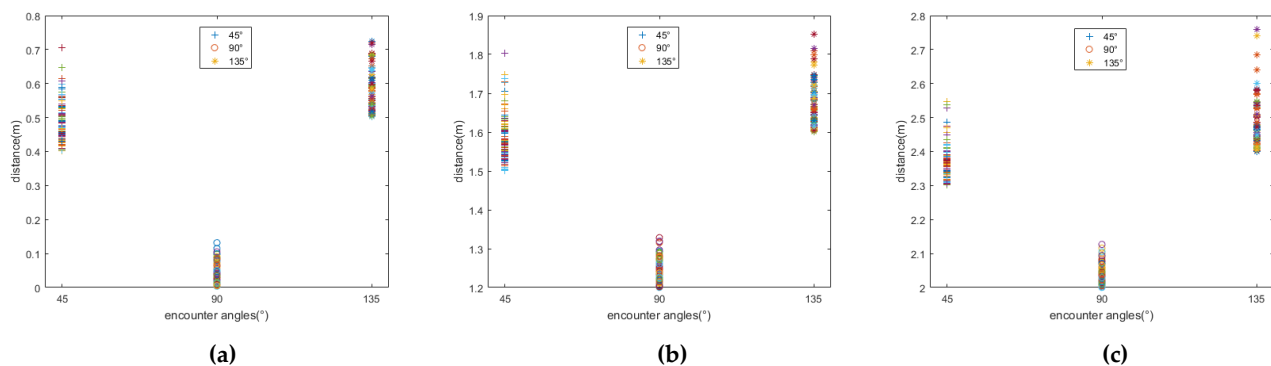


**FIGURE 22.** The shortest distance between lifeboat and ship side in irregular waves of a significant wave height 2.5m with initial distance of 1 time (a), 1.5 times (b), and 2 times (c) of lifeboat width. The horizontal ordinates respectively represent encounter angles  $45^\circ$ ,  $90^\circ$ , and  $135^\circ$  of main wave direction, and the longitudinal coordinates is the distance.

**FIGURE 23.** The shortest distance between lifeboat and ship side in irregular waves of a significant wave height 4m with initial distance of 1 time (a), 1.5 times (b), and 2 times (c) of lifeboat width. The horizontal ordinates respectively represent encounter angles 45°, 90°, and 135° of main wave direction, and the longitudinal coordinates is the distance.

**C. EXPERIMENTAL COMPARISON AT CROSS WAVES**

Under the condition of cross waves, the collision between the lifeboat and the ships is likely to happen. In this paper, the simulated experimental results of this condition are compared with the data of model tests in [11], and the initial conditions are consistent with those of Test 1 and 2 in [11]. The ship motion is consistent with the motion parameters, as shown in Figures 24 and 25.

The numerical results of our algorithm are compared with the data of model tests, as shown in Figures 26 and 27. The data in the figures are the curves of the position of the lifeboat with time. In Figures 26a and 26b, the maximum errors of the trajectory curve in the air are 0.58m and 1.32m, respectively. In Figures 27a and 27b, the maximum errors of the trajectory curve in the air are 0.56m and 1.11m, respectively.

The impacts are clearly visible in the graph of the accelerations in Figure 28. Both these impacts are actually a series of collisions where the lifeboat is exposed to impacts of low accelerations. This occurs since the ship first sways in the direction of the lifeboat motion and then towards the lifeboat at impact and the lifeboat is pushed on the shipside producing a series of impacts. These impacts can be seen in Figure 28a for both the experiments and simulations as a number of consecutive peaks in the horizontal accelerations. The error of the peak value is 1.6m/s<sup>2</sup>. The accelerations in the vertical directions at these impacts are low and are not even visible in Figure 28b.

In Test 2, the accelerations at impact against the mother ship are larger compared to Test 1. In the graph of the horizontal accelerations shown in Figure 29a, two distinct impacts can be seen for both the simulation and experiment. The simulated peaks occur slightly after their respective peaks in the experiment, because the irregular side of the ship is regarded as a plane. The error of the peak value is 1.0m/s<sup>2</sup>. It is apparent that the same situation occurs for both the simulation and experiment.

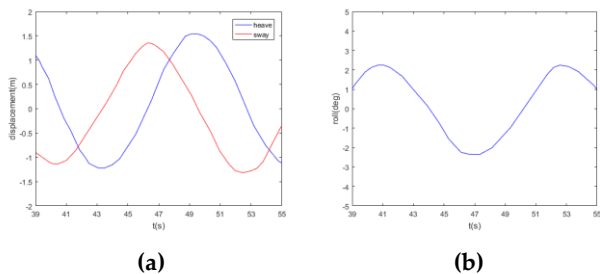


**FIGURE 24.** Ship motion parameters in test 1, (a) is heavy and sway, (b) is roll.

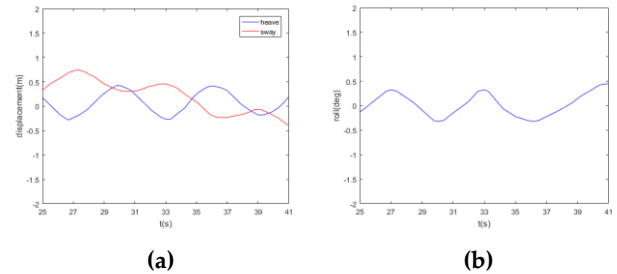


**FIGURE 25.** Ship motion parameters in test 2, (a) is heavy and sway, (b) is roll.

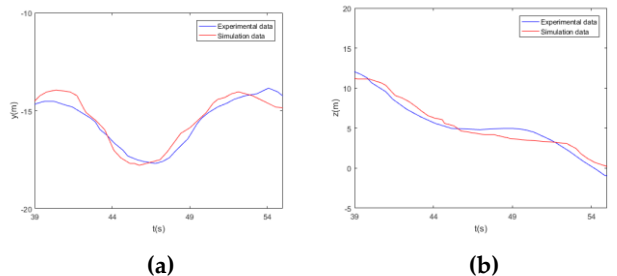


**FIGURE 26.** Comparison of lifeboat's trajectories with test 1, (a) and (b) are respectively the time-varying curves of the lifeboat's coordinates in the  $oy_1$  and  $oz_1$  axes.

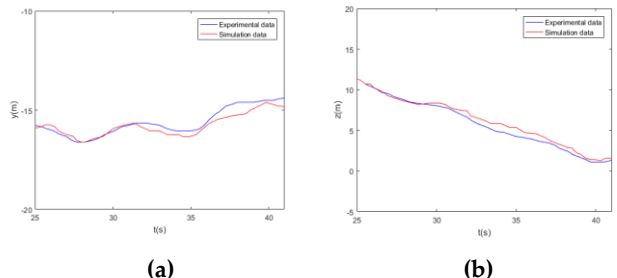


**FIGURE 27.** Comparison of lifeboat's trajectories with test 2, (a) and (b) are respectively the time-varying curves of the lifeboat's coordinates in the  $oy_1$  and  $oz_1$  axes.

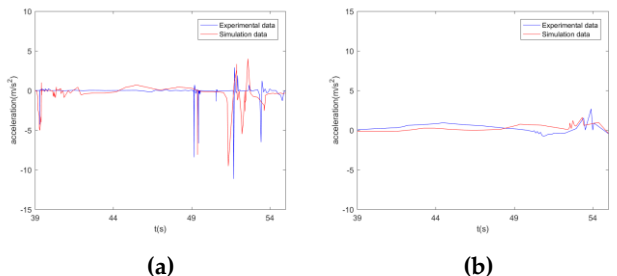
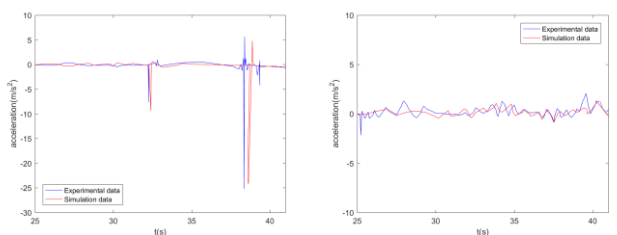


**FIGURE 28.** Comparison of lifeboat's acceleration with test 1, (a) and (b) are respectively the time-varying curves of the lifeboat's acceleration in the  $oy_1$  and  $oz_1$  axes.



(a) (b)

**FIGURE 29.** Comparison of lifeboat's acceleration with test 2, (a) and (b) are respectively the time-varying curves of the lifeboat's acceleration in the  $oy_1$  and  $oz_1$  axes.

#### IV. APPLICATION

This paper applies the established computational model to the software of three-dimensional simulation of the totally enclosed lifeboat. The software takes the container ship as physical prototype, and uses the 3ds Max to build a 3D models of the ship, lifeboat. The system constructs a virtual scene of releasing the lifeboat through three-dimensional virtual operation, as shown in the Figures 30 and 31.

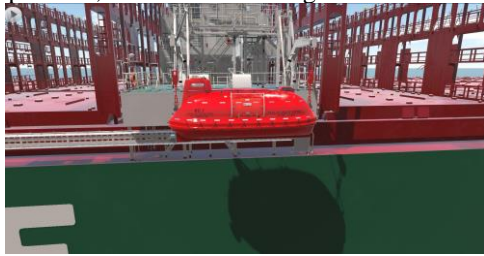


**FIGURE 30.** Scene of initial stage of lowering lifeboat.



**FIGURE 31.** Scene of the lifeboat reaching the surface of sea.

#### V. SUMMARY

This paper presents a multibody dynamics model for the totally enclosed lifeboat lowered from a ship, accounting for the coupled motion among the ship, lifeboat slings, cable-pulley system, and the lifeboat. The equations of the whole system are formulated by Kane's method. The numerical algorithm in this paper can simulate lowering a lifeboat in different speed of the cable released by the drum, and obtain the three-dimensional motion parameters of the ship, lifeboat, slings, pulleys, and the local tension load of the cable in the system. Thus, we present the following summaries:

1) Compared with the available model experimental results, the trajectories and acceleration of the lifeboat are close, and their trends are coincident. It can be concluded that our model is feasible. At present, there are few experiments available for comparison, and so we will make more efforts to apply our algorithm to ship structure design and manufacture. Even so, the computational model has been applied to the software of three-dimensional simulation of the totally enclosed lifeboat. It can be used to train crews to improve their proficiency in operation and safety awareness.

2) Oscillations can be seen to have occurred during lowering as the lifeboat swung as a pendulum. This is mainly due to the motions of the floating ship by the waves according to the experimental result. The motion of the ship has a significant effect on the lifeboat when the sea state is above level 4.

3) Under the conditions of cross waves, the collision between the lifeboat and the ship is likely to happen. The initial distance between the lifeboat and the ship is another important factor. It is safe that the initial distance is greater than 1.5 times the width of the lifeboat when the sea conditions are below level 5.

4) Due to the irregular shape of the lifeboat, ship, pulleys, etc., this paper cannot take the collisions among all the bodies into consideration, and so it is impossible to do simulation experiments under more severe environmental conditions accurately. For the motion of a particular ship, the model of MMG needs a lot of experimental data to get accurate hydrodynamic derivatives. When there is no experimental data for a ship, an accurate numerical algorithm is needed. The hydrodynamic force of the lifeboat is needed to be calculated accurately for the further research about the motion of the lifeboat on the sea. Shipwrecks often occur, and the lifeboat plays an important role in shipwrecks. Therefore, the motion model of the sinking ship needs to be studied in the future.

#### REFERENCES

- [1] J. K. N. Jr., P. J. Waugh, and A. J. Schweickhardt, "Injury criteria of the IMO and the Hybrid III dummy as indicators of injury potential in free-fall lifeboats," *OCEAN ENG*, vol. 23, no. 5, pp. 385-401, Jul. 1996. DOI: 10.1016/0029-8018(95)00041-0
- [2] R. Billard, J. Smith, and B. Veitch, "Assessing Lifeboat Coxswain Training Alternatives Using a Simulator," *J NAVIGATION*, pp.1-16, 2019. DOI: 10.1017/S0373463319000705
- [3] Y. Luo, J. C. Trickey, C. E. James, and R. L. Jack, "Lifeboat launch simulation and its application to safety assessment," in *Proc. Annu. Offshore Technol. Conf*, Houston, TX, United states, 1992, pp.503-512 10.4043/6929-MS
- [4] A. J. S. Re and B. Veitch, "Evacuation Performance of Davit Launched Lifeboats," in *Proc Int Conf Offshore Mech Arct Eng - OMAE*, Vancouver, BC, Canada, 2004, pp. 487-494.
- [5] A. J. S. Re and B. Veitch, "A comparison of three types of evacuation system," *Trans Soc Nav Archit Mar Eng*, vol. 115, pp. 119-139, 2007.
- [6] A. J. S. Re, B. Veitch, and D. Pelley, "Systematic investigation of lifeboat evacuation performance," *Trans Soc Nav Archit Mar Eng*, vol. 110: pp. 341-360, 2002.
- [7] A. J. S. Re, J. Antonio, B. Veitch, S. Mulrooney, and T. Hopkins, "Systematic Experimental Evaluation of Lifeboat Evacuation Performance in a Range of Environmental Conditions: Phase I," Institute for Marine Dynamics, St. John's, NL, CA, Tech. Rep. TR-2002-02, 2002.
- [8] D. Pelley, "Performance of twin falls davit & lifeboat evacuation system in extreme seas," M.S. thesis, Dept. Engineering and Applied Science, MUN Univ., St. Johns, NL, Canada, 2003.
- [9] C. Magluta, N. Roitman, and R. C. Batista, "Dynamic behaviour analysis of a lifeboat system under simulated accidents," *Mech Syst Signal Process*, vol. 10, no. 6, pp. 763-774, Nov. 1996. DOI: 10.1006/mssp.1996.0051
- [10] W. Raman-Nair, A. S. Re, and B. Veitch, "Dynamics of Lifeboat and Boom in Deployment from a Moving Support," *MULTIBODY SYST DYN*, vol. 13, no. 3, pp. 267-298, Apr. 2005. DOI: 10.1007/s11044-005-4084-4
- [11] P. Ekman, "A numerical model to simulate launching of evacuation capsules from a ship in beam seas - Simulations and validation using experimental tests," *Int Shipbuild Progr*, vol. 53, no. 2, pp. 83-102, 2006.

- [12] P. Ekman, "Numerical Study of a Method to Reduce Rescue Boat Motions during Launching from a Ship in Waves," *MAR SYST OCEAN TECHNOL*, vol. 1, no. 2, pp. 91-97, Jun. 2005. DOI. 10.1007/BF03449199
- [13] P. Dymarski and C. Dymarski, "Computational model for simulation of lifeboat motions during its launching from ship in rough seas," *POL MARIT RES*, vol. 19, no. 3, pp. 45-52, Oct. 2012. DOI.10.2478/v10012-012-0030-6
- [14] C. Dymarski, P. Dymarski, and A. Kniat, "Searching for Critical Conditions During Lifeboat Launching – Simulations," *POL MARIT RES*, vol. 24, no. s1, pp. 53-58, Oct. 2017. DOI.10.1515/pomr-2017-0021
- [15] A. Kniat, Visualization of a Lifeboat Motion During Lowering Along Ship's Side. *POL MARIT RES*, vol. 24, no. 4, pp. 42-46, Dec. 2017. DOI. 10.1515/pomr-2017-0134
- [16] T. Anurakpandit, N. C. Townsend, and P. A. Wilson, "The numerical and experimental investigations of a gimbal pendulum energy harvester," *Int J Non Linear Mech*, vol.120, Apr. 2020. DOI. 10.1016/j.ijnonlinmec.2019.103384
- [17] J. Cuadrado, J. Cardenal, and E. Bayo, "Modeling and Solution Methods for Efficient Real-Time Simulation of Multibody Dynamics," *MULTIBODY SYST DYN*, vol. 1, no. 3, pp. 259-280, Jan. 1997. DOI.10.1023/A:1009754006096
- [18] W. Raman-Nair and R. E. Baddour, "Three-Dimensional Dynamics of a Flexible Marine Riser Undergoing Large Elastic Deformations," *MULTIBODY SYST DYN*, vol. 10, no. 4, pp. 393-423, Nov. 2003. DOI. 10.1023/A:1026213630987
- [19] W. Raman-Nair and B. Colbourne, Dynamics of a mussel longline system. *AQUACULT ENG*, vol. 27, no. 3, pp. 191-212, Mar. 2003. DOI. 10.1016/S0144-8609(02)00083-3
- [20] T. R. Kane, P. W. Likins, and D. A. Levinson, *Spacecraft Dynamics*, McGraw Hill Inc., New York, USA 1983, pp.30
- [21] K. L. Johnson, *Contact Mechanics*. Cambridge University Press: Cambridge, the United Kingdom, 1985, pp. 84-104.
- [22] W. Raman-Nair and S. N. Chin, "Estimation of impact forces between small bodies in waves," *OCEAN ENG*, vol. 46, pp. 46-51, June 2012. DOI.10.1016/j.oceaneng.2012.03.001
- [23] H. M. Lankarani and P. E. Nikravesh, "Continuous contact force models for impact analysis in multibody systems," *NONLINEAR DYNAM*, vol. 5, no. 2, pp. 193-207, Mar. 1994. DOI.10.1007/BF00045676
- [24] X. JIA, and Y. YANG, *Ship motion mathematical model: the mechanism modeling and identification modeling*; Dalian Maritime University press: Dalian, China, 1999, pp. 49-138.  
贾欣乐, 杨盐生. 船舶运动数学模型—机理建模与辨识建模[M]. 大连海事大学出版社, 大连, 中国, 1999, 49-138.
- [25] J. Mo, "Numerical simulation of ship maneuvering motion with six degree of freedom in waves," M.S. thesis, Dept. Design and Construct of Naval Architecture and Ocean Structure, Harbin Engineering Univ., Harbin, China, 2009.  
莫建. 波浪中船舶六自由度操纵运动数值仿真[D].硕士学位论文, 船舶与海洋结构物设计与制造, 哈尔滨工程大学, 中国, 2009.
- [26] S. Qiu, H. Ren, and H. Li, "Computational Model for Simulation of Lifeboat Free-Fall during Its Launching from Ship in Rough Seas," *J MAR SCI ENG*, vol. 8, no. 9, pp. 631, 2020. DOI.10.3390/jmse8090631
- [27] K. Kimura, S. Takahashi, and K. Tanimoto, "Stability of rubble mound foundations of composite breakwaters under oblique wave attack". in *Proc 24 Int Conf Coastal Energy Kobe*, Hiragishi Sapporo, Japan, 1994, pp. 1227-1240.
- [28] Y. Goda, *Random Sea and Design of Maritime Structures*; University of Tokyo Press: Tokyo, Japan, 1985, pp. 31-32.
- [29] L. Changhoon, J. Jae-Sang, and H. Merrick C, "Asymmetry in Directional Spreading Function of Sea Waves Due to Refraction". in *Proc Int Conf Offshore Mech Arct Eng – OMAE*, Honolulu, HI, United states, 2009, pp. 415-423.
- [30] Q. Xiaobin, Y. Yong, Z. Xiufeng, and L. ye, "Influence of irregular disturbance of sea wave on ship motion," *Jiaotong Yunshu Gongcheng Xuebao*, vol.16, no.3, pp. 116-124, June, 2016.  
钱小斌, 尹勇, 张秀凤, 李业. 海上不规则波浪扰动对船舶运动的影响. 交通运输工程学报, 16,3,116-124, 6月, 2016.
- [31] C. Sun, W. He, and J. Hong, "Neural Network Control of a Flexible Robotic Manipulator Using the Lumped Spring-Mass Model," *IEEE T SYST MAN CYB*, vol. 47, no. 8, pp. 1863-1874, Aug. 2017. DOI.10.1109/TSMC.2016.2562506
- [32] N. Mitsui and K. Hirahara, "Simple Spring-mass Model Simulation of Earthquake Cycle along the Nankai Trough in Southwest Japan," *PURE APPL GEOPHYS*, vol. 161, no. 11, pp. 2433-2450, Jan. 2004. DOI.10.1007/s00024-004-2574-6
- [33] S. Jean, H. Richard, Q. Jacques, B. Véronique, and H. Christine, "Changes in spring-mass model parameters and energy cost during track running to exhaustion," *J STRENGTH COND RES*, vol. 22, no. 3, pp. 930-936, 2008. DOI.10.1519/JSC.0b013e31816a4475
- [34] F. Ju and Y. S. Choo, "Super element approach to cable passing through multiple pulleys," *INT J SOLIDS STRUCT*, vol. 42, no. 11-12, pp. 3533-3547, Jun. 2005. DOI.10.1016/j.ijsolstr.2004.10.014
- [35] I. García-Fernández, M. Pla-Castells, and R. J. Martínez-Durá, "Elevation Cable Modeling for Interactive Simulation of Cranes," in *8th ACM SIGGRAPH/Eurographics Symposium on Computer Animation, SCA 2008*, Dublin, Ireland, 2008. DOI.10.2312/SCA/SCA08/173-181
- [36] J. W. Kamman and R. L. Huston, "Multibody Dynamics Modeling of Variable Length Cable Systems," *MULTIBODY SYST DYN*, vol. 5, no. 3, pp. 211-221, 2001. DOI. 10.1023/A:1011489801339
- [37] Z. Qi, J. Wang, and G. Wang, "An efficient model for dynamic analysis and simulation of cable-pulley systems with time-varying cable lengths," *MECH MACH THEORY*, vol. 116, pp. 383-403, Oct. 2017. DOI.10.1016/j.mechmachtheory.2017.06.009
- [38] J. Wang, Z. Qi, and G. Wang, "Hybrid modeling for dynamic analysis of cable-pulley systems with time-varying length cable and its application," *J SOUND VIB*, vol. 406, pp. 277-294, Oct. 2017. DOI. 10.1016/j.jsv.2017.06.024.
- [39] Z. Kan, F. Li, H. Peng, B. Chen, and X. Song, "Sliding cable modeling: A nonlinear complementarity function based framework," *Mech Syst Signal Process*, vol. 146, pp. 1-20, Jan. 2021. DOI.10.1016/j.ymsp.2020.107021
- [40] B. W. Oppenheim and P. A. Wilson, "Static 2-D solution of a mooring line of arbitrary composition in the vertical and horizontal operating modes," *Int Shipbuild Prog*, vol.29, no. 334, pp.142-153, Feb. 1982. DOI. 10.3233/ISP-1982-2933401.
- [41] A. J. S. Re and B. Veitch, "Experimental evaluation of lifeboat evacuation performance," *Trans. Society of Naval Architects and Marine Engineers*, vol.109, pp.18, 2001.



### SHAORYANG QIU

was born in Liaoning Province, China in 1992. received the B.E. and M.S. degrees in traffic and transportation engineering from Dalian Maritime University, Dalian, China, in 2014 and 2016, respectively, where he is currently pursuing the Ph.D.

degree in traffic information engineering and control with the Key Laboratory of Marine Dynamic Simulation and Control for Ministry of Communications. His research interests are virtual reality, multibody dynamics, and ship motion modeling. Email:qsydmu@163.com.

related to ship intelligence. Email:zhouyi@cnooc.com.cn



### DELONG WANG

was born in Heilongjiang Province, China in 1986. received the Ph.D. degree in traffic and transportation engineering from the Key Laboratory of Marine Simulation & Control for Ministry of Communications, Dalian Maritime University of China in 2018. His research interests include ship collision avoidance, ship behavior, intelligent assessment. Email :

wangdelong1986@sina.com



### HONGXIANG REN

was born in Heilongjiang Province, China in 1974. He received the Ph.D. degree from the Key Laboratory of Marine Simulation & Control for Ministry of Communications, Dalian Maritime University of China in 2009. He is currently a member of the China Image and Graphics Society, a member of the China System Simulation Society, a member of the China Navigation Society. His research

interests include virtual reality, visual simulation and computer graphics. Email : dmuhx@163.com.



### HAIJIANG LI

was born in Hebei Province, China in 1991. received the B.E. and M.S. degrees in traffic and transportation engineering from Dalian Maritime University, Dalian, China, in 2013 and 2015, respectively, where he is currently pursuing the Ph.D. degree in traffic information engineering and control with the Key Laboratory of Marine

Dynamic Simulation and Control for Ministry of Communications. His research interests are virtual reality, computer graphics, deep learning, and data mining. Email : hai\_nav@163.com.



### YI ZHOU

was born in Tianjin, China in 1985. received the B.E. and B.S. degrees in mechanical engineering from Huaihai Institute of Technology (Now it is Jiangsu Ocean University), Jiangsu, China, in 2008 He is currently working at CNOOC, where he is engaged in research